Evolution of the northern Sierra Nevada metamorphic belt: Petrological, structural, and Ar/Ar constraints

BRADLEY R. HACKER *Department of Geology, Stanford University, Stanford, California 94305-2115*

ABSTRACT

The Sierra Nevada metamorphic belt constitutes an important record of the growth of continental crust from essentially oceanic materials. In the northern Sierra, the central part of the belt is made up of volcanoplutonic arcs and sediment-dominated units inferred to be accretionary wedges or closed ocean basins. The latter are broken formation and mélange composed of radiolarian chert, lava, and volcanogenic and continental turbidites. Sedimentary detritus in the largest of these units can be plausibly linked to sources farther east in the Sierra, suggesting that deposition occurred near the eastern Sierran arc. Isoclinal folds, steeply dipping foliations, and steeply plunging down-dip lineations are characteristic structures. The westernmost unit is only feebly recrystallized, and deformation was accomplished principally by stress solution and local redeposition in veins. More easterly, inboard units are compositionally similar, but they recrystallized at pumpellyite-actinolite– and blueschist-facies conditions and deformed via solution-transfer and dislocation creep. Phengite silica contents, the degree of quartz veining, and the locations of pseudo-isograds support an eastward increase in metamorphic pressure and temperature. Metamorphic conditions during the growth of pumpellyite and actinolite ranged from ~150–350 °C and 200–400 MPa, compatible with recrystallization and deformation in subduction zones or the deeper levels of magmatic arcs. Ar/Ar ages of volcaniclastic rocks and crosscutting plutons constrain the age of deformation and metamorphism in the western part of the region to 174–165 Ma. Deformation and recrystallization in more easterly units may have been coeval or begun as early as Triassic time.

INTRODUCTION AND REGIONAL GEOLOGY

Extensive geologic investigations and large areal extent make the Sierra Nevada/Klamath Mountains orogen an archetype of continental growth via long-term subduction of oceanic lithosphere. The so-called "Central belt" (Fig. 1) has been the most difficult metamorphic unit in the Sierra Nevada to understand, and yet its large outcrop area and central location—between terranes of the western and eastern Sierra Nevada—make it a linchpin for the entire orogen. Key to unraveling the tectonic history of these rocks is determining the sources and ages of volcanic and sedimentary rocks and the conditions and ages of metamorphism and deformation. Although there is evidence of deformation and metamorphism in the northern Sierra Nevada prior to, and coincident with, the Nevadan orogeny (middle Late Jurassic), the pressure-temperature conditions, tectonic settings, and ages of these events are poorly constrained (Day and others, 1988). Equally important is understanding the genesis of widespread mélange and broken formation in the Central belt. The units have been referred to as "known mélange" (Schweickert and Cowan, 1975, p. 1330), "largely chaotic (?) upper Paleozoic to Mesozoic" rocks, and "one of the most enigmatic" terranes (Schweickert, 1981, p. 123 and 124). This paper addresses these issues for the Yuba River drainage (Fig. 2A), using field work, back-scattered electron microscopy, electron-probe microanalysis, and Ar isotopes.

METHODS OF INVESTIGATION

The fine grain size of these low-grade rocks made analysis by conventional thin-section petrography problematic. Consequently, emphasis was placed on identifying minerals, foliations, and sequences of metamorphic and deformational events by back-scattered electron microscopy (BSEM) and electron-probe microanalysis (EPMA). Back-scattered electron imaging and electron probe analytical details are provided by Hacker and others (1992).

Equilibrium mineral assemblages can be difficult to identify in low-grade rocks, and a brief discussion of techniques used is warranted. This is particularly true for trace sulfide and oxide minerals, which are nearly always euhedral, and rarely in contact. Widespread relict igneous and sedimentary phases indicate that complete textural and chemical equilibrium was often not attained, except in tuffaceous units where recrystallization was pervasive. A combination of techniques was used to identify equilibrium mineral assemblages, including (1) recognizing phases in contact without signs of reaction, (2) recognizing a group of phases replacing a single relict phase, (3) identifying incompatible phases, (4) identifying violations of the phase rule, and (5) observing systematic partitioning of elements among phases. Most samples contain high-variance assemblages that are not useful for constraining conditions of metamorphism or identifying reaction relationships among assemblages. Samples that contain low-variance assemblages are emphasized in the following discussion. Particular care was taken to determine whether individual phases predated, postdated, or were an integral part of deformation fabrics.

The Ar isotopic measurements were conducted at Stanford on mineral separates prepared by standard heavy liquid and gravity/magnetic separation methods. The separates are very pure; because they were only a few milligrams, every grain was examined with a microscope, and undesired phases were picked out by hand. The samples were loaded into aluminum-foil packets and irradiated at the USGS TRIGA reactor in Denver. Gas was extracted in 8-min periods with a double-vacuum (Staudacher-type) resistance furnace with a Ta crucible and replaceable Mo liner. Extracted gas was equilibrated with SAES Zr-Al getters for 5 min, and analyzed with a MAP 216 mass spectrometer for 10 min. Dynamic and static blanks of ^{40}Ar at 1200 °C were typically 2.4×10^{-15} and 1.2×10^{-17} moles. Isotopic abundances were calculated by linear extrapolation to time zero of peak heights above background during six serial scans of ^{40}Ar to ^{36}Ar. These data were corrected for neutron flux gradients (using sani-

Geological Society of America Bulletin, v. 105, p. 637–656, 14 figs., 4 tables, May 1993.

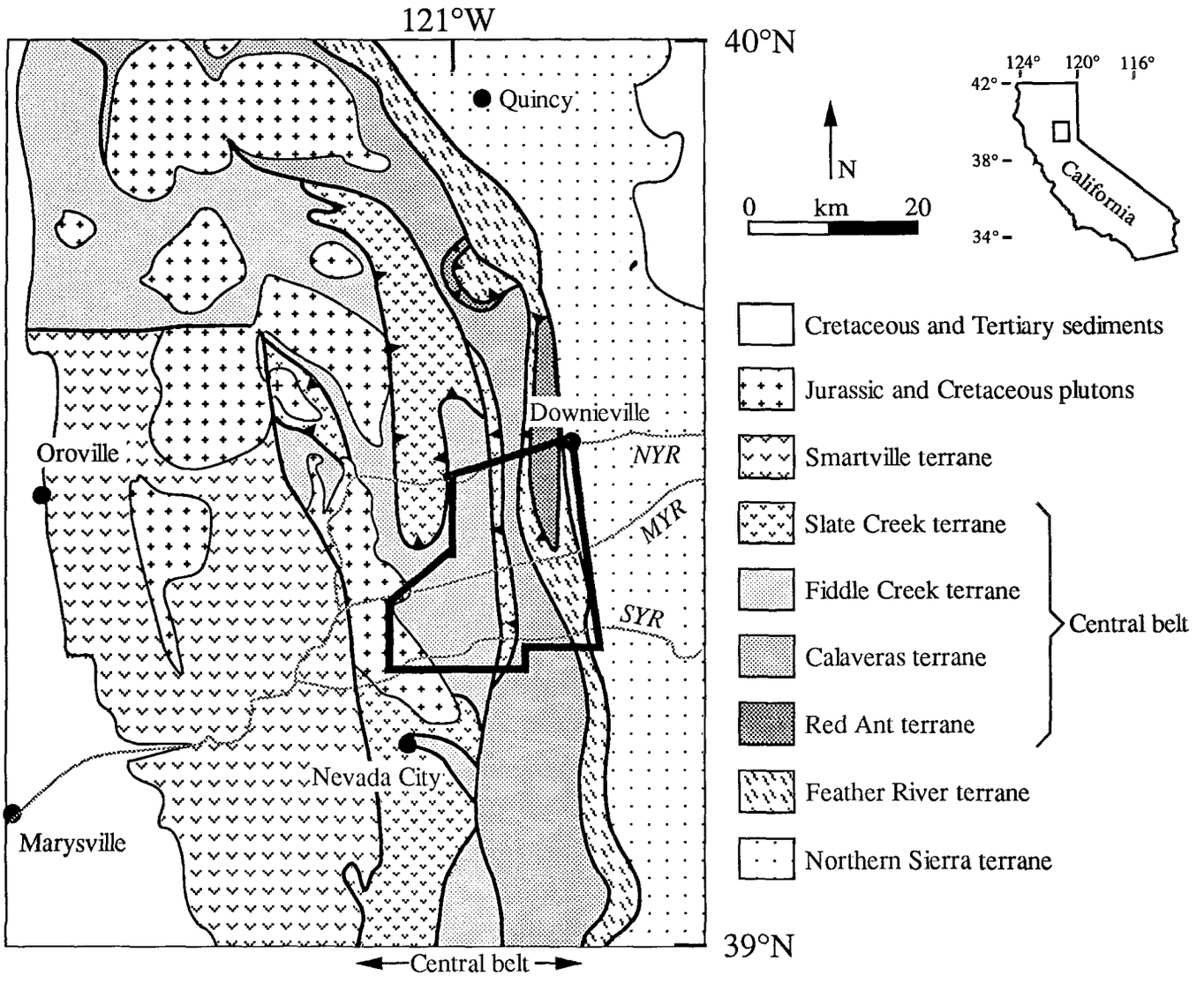

Figure 1. Tectonic map of the northern Sierra Nevada metamorphic belt. Outline shows area of Figure 2.

dine standard 85G003 with an assumed age of 27.92 Ma), decay since irradiation, and interference of Ca- and K-produced Ar isotopes. Reported uncertainties are one-sigma determined using uncertainties in monitor age, decay rates of ^{37}Ar, ^{39}Ar, and ^{40}K, rates of reactor-produced Ar isotopes, duration of irradiation, time between irradiation and analysis, peak heights, blank values, and irradiation parameter J. The time scale of Harland and others (1989) is used throughout, except for Hodych and Dunning's (1992) age of 202 ± 1 Ma for the Jurassic-Triassic boundary.

FIELD RELATIONS AND PETROGRAPHY

Metamorphic rocks in the northern Sierra Nevada were divided by Edelman and others (1989b) into seven units with different structural, metamorphic, and/or depositional histories. In general, the units dip steeply eastward and form a stack of west-directed thrust sheets. Detailed lithologic and regional descriptions were given by Hietanen (1981) and Edelman and others (1989b); the following is a brief summary of units in the Yuba River area shown in Figure 2A. The Slate Creek terrane is a Late Triassic immature intraoceanic arc (Edelman and others, 1989a; Saleeby and others, 1989). The Fiddle Creek, Calaveras, and Red Ant terranes include Mesozoic to Paleozoic broken formation and mélange interpreted to have formed during diachronous subduction (Hietanen, 1981; Sharp, 1988; Hacker and Goodge, 1990). The Feather River terrane has been interpreted as a disrupted, polygenetic Paleozoic ophiolite (Edelman and others, 1989b; Hacker and Peacock, 1990). The Northern Sierra terrane (Fig. 1) is composed of early Paleozoic metasedimentary rocks of the Shoo Fly Complex that are overlain by a Devonian-Jurassic magmatic arc sequence (Harwood, 1988). The Smartville terrane (Fig. 1) is a Middle Jurassic rifted magmatic arc (Beard and Day, 1987) that formed within Early Jurassic basement (Edelman and others, 1989a; Saleeby and others, 1989). Thus, the continental crust in this part of the Sierra Nevada has been built from chiefly volcanoplutonic arcs and ocean-basin– and continent-derived sediments.

Terranes in the Yuba River area are juxtaposed along three systems of faults (Fig. 2A) that were active at different times (Edelman and others, 1989b). Edelman and others (1989b) inferred that the Fiddle Creek, Cala-

veras, Red Ant, and Feather River terranes were juxtaposed along east-dipping thrust faults prior to Middle Jurassic time; the Feather River/Red Ant fault is the only one of these faults exposed in the Yuba River area. The Slate Creek terrane is hypothesized to have been thrust eastward over these amalgamated terranes along the west-dipping Slate Creek thrust after the ca. 200 Ma genesis of the Slate Creek terrane and prior to crystallization of the 168 Ma Scales pluton (Edelman and others, 1989a). The conspicuous, throughgoing Gillis Hill, Goodyears Creek, and Downieville faults are Nevadan (middle Late Jurassic), steeply east-dipping reverse faults that offset or reactivate the early thrust faults (Edelman and others, 1989b).

Feather River Terrane

The Feather River terrane is a heterogeneous assemblage of rocks less than 10 km wide that stretches more than 150 km southward from the north end of the Sierra Nevada. It contains all of the requisite units of an ophiolite: ultramafic rocks, massive and layered gabbro, sheeted dikes, pillow lava, chert, and Fe-rich sedimentary rock. P, Ti, Y, and Zr abundances indicate a mid-ocean-ridge basalt protolith for some mafic rocks (Hietanen, 1981), but the Feather River terrane does not represent normal mid-ocean-ridge lithosphere (Hacker and Peacock, 1990). A broad spectrum of Devonian to Permian Pb/U, Ar/Ar, and K/Ar ages (see summary in Hacker and Peacock, 1990), suggests that the Feather River terrane is polygenetic. Structural disruption of the terrane, including folding and imbrication with adjacent units, has occurred, but widespread mélange or broken formation are absent. The Feather River terrane was metamorphosed three times: an early greenschist-facies event was followed by amphibolite-facies recrystallization, and then by pumpellyite-actinolite–facies metamorphism (Hacker and Peacock, 1990). The characteristic metamorphism was the amphibolite-facies event, which occurred in a Paleozoic magmatic arc (Hacker and Peacock, 1990). The previously unrecognized pumpellyite-actinolite–facies event is described here in detail because this metamorphism is shared with other terranes in the Yuba River area.

The amphibolite-facies minerals in mafic meta-igneous rocks (hornblende, plagioclase, garnet, quartz, muscovite, biotite, and ilmenite) were weakly recrystallized and deformed during the pumpellyite-actinolite facies metamorphism (Fig. 3). Low-variance mineral assemblages are listed in Table 1. Actinolite rims hornblende crystals, and pumpellyite and chlorite are present along cracks in hornblendes. Plagioclase grains are replaced by albite + pumpellyite, albite + epidote, albite + phengite, or rarely actinolite + chlorite. Micas are commonly replaced by chlorite + pumpellyite, phengite + pumpellyite + sphene, and rarely by chlorite + epidote. Rare stilpnomelane occurs as overgrowths on actinolite and mica. Veins of albite + actinolite, albite + chlorite + quartz, albite + calcite, pumpellyite + pyrite + sphene, and epidote + chlorite also cut across the amphibolite-facies minerals. Sphene is a partial replacement of ilmenite, and hematite is frequently an alteration product of magnetite.

The amphibolite-facies assemblage in sedimentary rocks (garnet + quartz + biotite + muscovite + plagioclase) was also overprinted by the pumpellyite-actinolite facies metamorphism. Garnets are surrounded by several-micron-wide rims of unoriented phengite crystals. Biotite and muscovite grains are replaced by phengite + sphene, chlorite + sphene, chlorite + pumpellyite, or rarely epidote. The pumpellyite crystals are elongate parallel to the mica cleavage, and some contain thin skeletons of allanite or ilmenite. Some chlorite crystals are overgrown by stilpnomelane. Plagioclase is altered to albite + pumpellyite + phengite. Veins of quartz + pumpellyite, albite + actinolite + quartz, and albite + chlorite + quartz formed concurrently with the pumpellyite-actinolite facies parageneses in the rock matrix. Hematite is a typical alteration product of magnetite.

Deformation coincident with amphibolite-facies metamorphism produced a foliation, lineation, and folds. More recent deformation is minor by comparison. Aside from mineral-filled fractures and faults of centimeter-scale offset, structures associated with the pumpellyite-actinolite facies metamorphism have not been recognized.

Red Ant Terrane

The Red Ant terrane is a subduction zone assemblage that consists of metavolcanic blocks enclosed in predominantly metasedimentary rock (Schweickert and others, 1980). It contains primarily pumpellyite-actinolite facies assemblages and locally developed epidote-glaucophane parageneses (Table 1; Hacker and Goodge, 1990). Textures described below indicate that the pumpellyite-actinolite minerals grew on the blueschist assemblages.

The metasedimentary rocks consist of strongly attenuated and folded interbedded chert and argillite cut by strongly folded quartzose veins (Fig. 3b in Hacker and Goodge, 1990). Quartz and phengite are the dominant metamorphic phases, and sphene, chlorite, albite, calcite, stilpnomelane, epidote, magnetite, and hematite occur locally. Rare sodic amphibole and lawsonite are present. Phengite, sodic amphibole, and lawsonite crystals are folded, indicating prekinematic growth. Radiating aggregates of stilpnomelane grown on relict rutile cut across folded micaceous layers. The quartzose veins (quartz + albite + chlorite) comprise a complete spectrum of earlier strongly folded veins that cut across folded micaceous layers, and later weakly folded veins that cut across folded micaceous layers and earlier veins, indicating that quartz, albite, and chlorite were recrystallizing during the folding.

Interlayered with the metasediments are volcanogenic sandstone and tuff—strongly folded, fine-grained schists composed of alternating centimeter-thick quartzose and volcanogenic layers. The volcanogenic layers contain subassemblages of actinolite + albite + microcline + phengite + chlorite + sphene + quartz + pumpellyite + epidote + lawsonite (Fig. 4). Euhedral volcanic plagioclase crystals are partially replaced by chlorite + rutile + epidote or albite ± epidote. Relict euhedral clinopyroxene crystals are partially replaced by stilpnomelane. Mats of chlorite crystals contain numerous micron-sized crystals of sphene, albite, euhedral to subhedral porphyroblastic epidote, and phengite. In some rocks, the actinolite crystals form overgrowths on sodic amphiboles, which are themselves overgrowths on igneous hornblende crystals. Randomly oriented veins filled with albite + calcite or albite + chlorite + epidote are common.

Metamorphosed volcanic breccias preserve textural evidence which indicates that blueschist-facies metamorphism preceded pumpellyite-actinolite facies metamorphism. Breccia fragments initially contained igneous plagioclase, pyroxene, quartz, and perhaps K-feldspar phenocrysts, in a finer-grained groundmass. The plagioclase phenocrysts have since recrystallized to albite, the pyroxene crystals are replaced by chlorite, and the groundmass has been altered to chlorite, sphene, and minor quartz. The stable blueschist-facies assemblage in the fragments was probably albite + epidote + chlorite + sphene + quartz. The breccia matrix contains the equilibrium blueschist-facies assemblage: albite + epidote + chlorite + sphene +

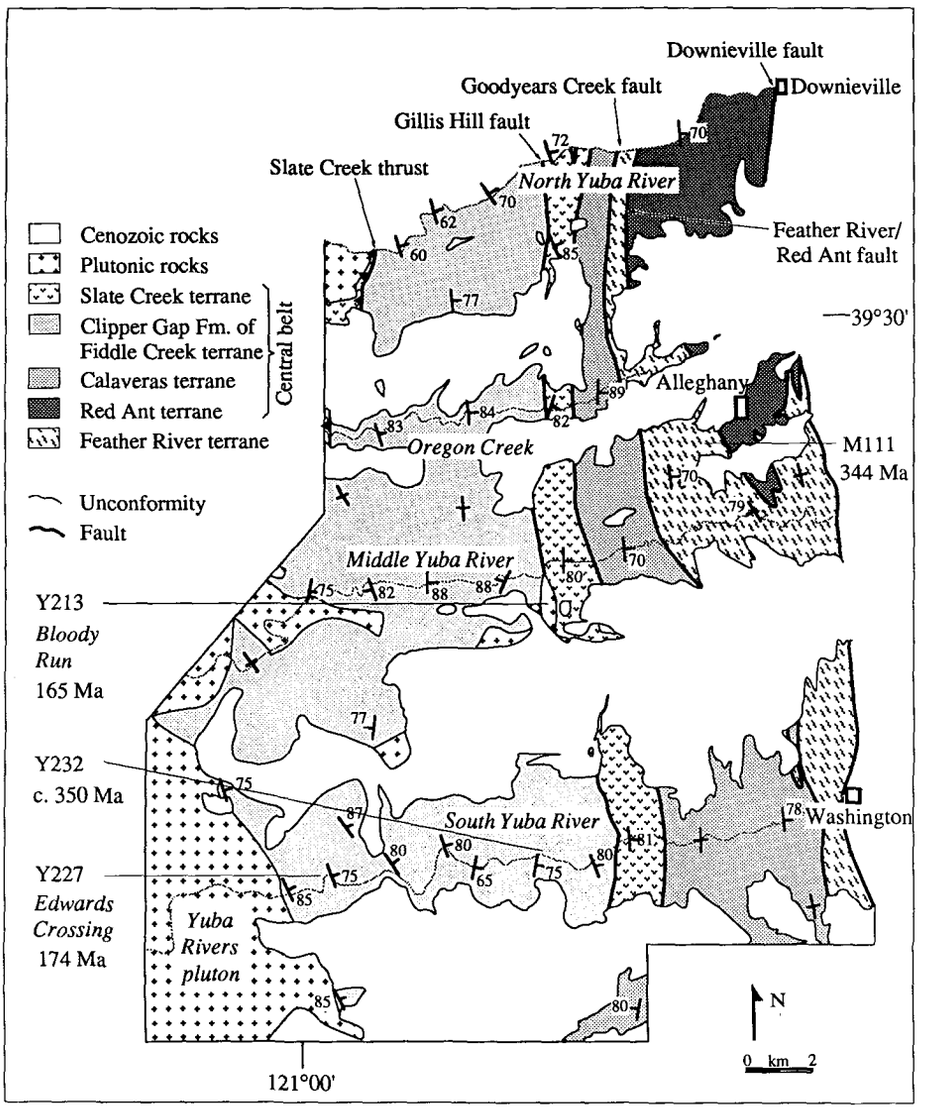

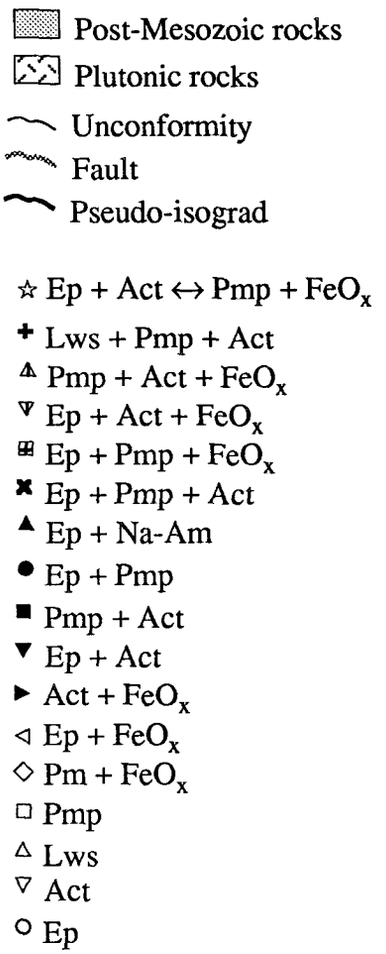

Explanation for Figure 2B.

Figure 2A. Geologic map of the Yuba River area. The locations of samples that were examined by back-scattered electron microscopy (BSEM) and electron-probe microanalysis (EPMA) are shown by circles; more than 200 other samples were examined in thin section. The density of samples from the Clipper Gap unit examined by BSEM and EPMA is less than the other units because metamorphic recrystallization is limited.

phengite + quartz + sodic amphibole + magnetite.

The volcanic breccias are undeformed except for two stages of veining. Early veins contain nematoblastic sodic amphibole, phengite, sphene, albite, chlorite, lawsonite, epidote, and minor quartz (Fig. 7c in Hacker and Goodge, 1990). The lawsonite forms rare cores to epidote crystals, and it is not clear whether lawsonite and sodic amphibole grew together, or whether epidote replaced lawsonite during growth of sodic amphibole. The shape of epidote crystals in early veins is influenced by the orientations of adjacent sodic amphibole crystals, *suggesting* that epidote was stable with sodic amphibole. The porphyroblastic habit of most epidote crystals, however, precludes determining whether epidote was part of the earliest mineral assemblages. Later veins contain albite, iron-rich chlorite, calcite, epidote, sphene, phengite, hematite, and actinolite rims grown on sodic amphiboles. Within the breccia fragments, fibrous bundles of actinolite grew on chlorite, radiating sheaves of stilpnomelane grew within chlorite, and epidote crystallized in veins. Strain shadows filled with stilpnomelane + quartz developed in the breccia matrix around pyrite crystals.

The simplest interpretation of the textural relationships in the volcanic breccias is that early blueschist-facies assemblages were albite + chlorite + sphene + phengite + epidote + sodic amphibole + quartz + magnetite in the matrix, albite + chlorite + sphene + quartz + epidote in the fragments, and albite + chlorite + sphene + phengite + sodic amphibole + epidote + quartz in the early veins. Later pumpellyite-actinolite facies assem-

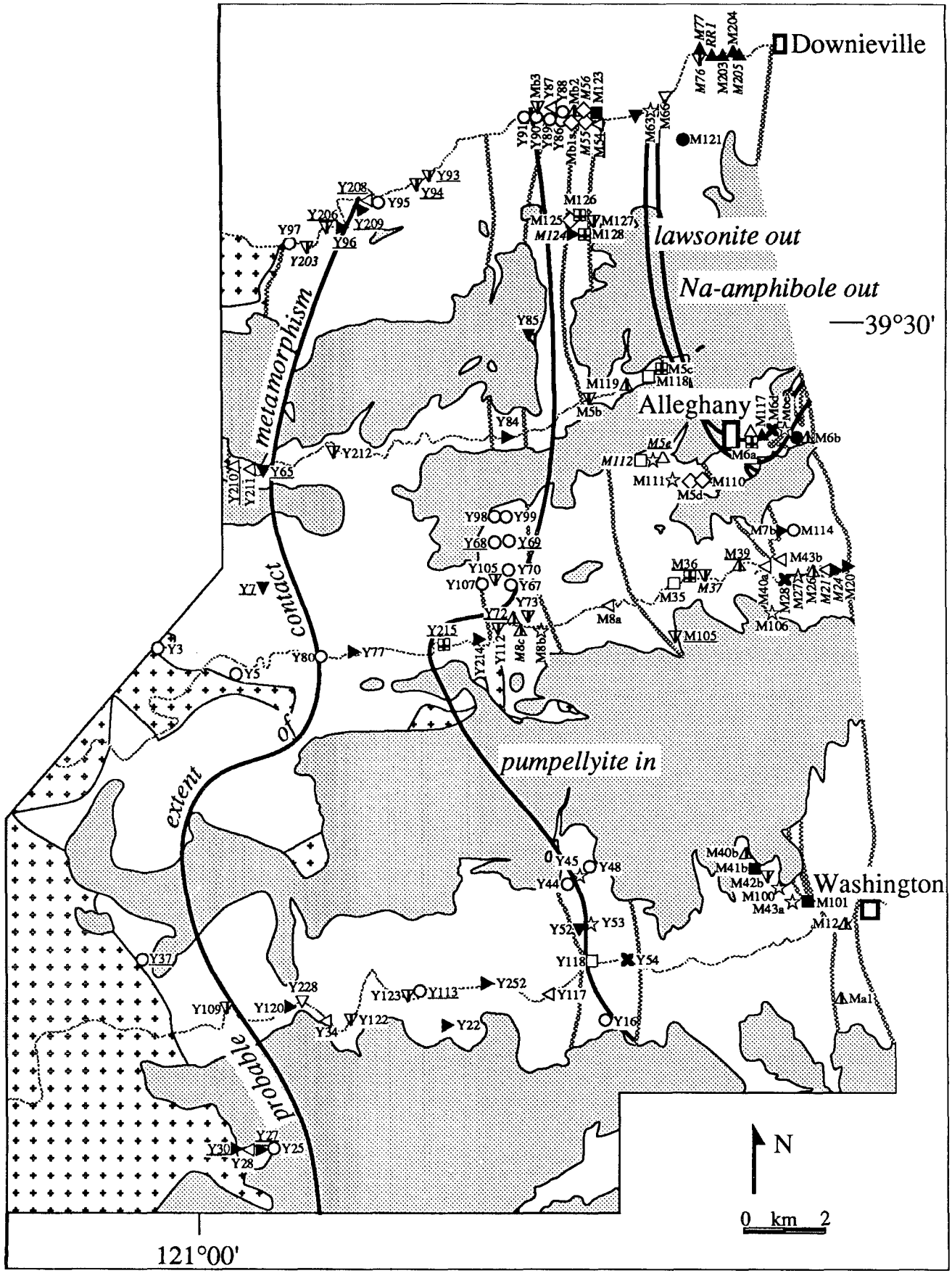

Figure 2B. Locations of samples containing key metamorphic minerals. Underlined or italicized samples contain biotite or stilpnomelane, respectively. The lawsonite outcrop west-southwest of Alleghany in the Feather River terrane is an outlier of the Red Ant terrane that is too small to show at this scale. Much of the epidote and biotite shown near plutonic rocks in the Clipper Gap Formation is likely a result of contact metamorphism.

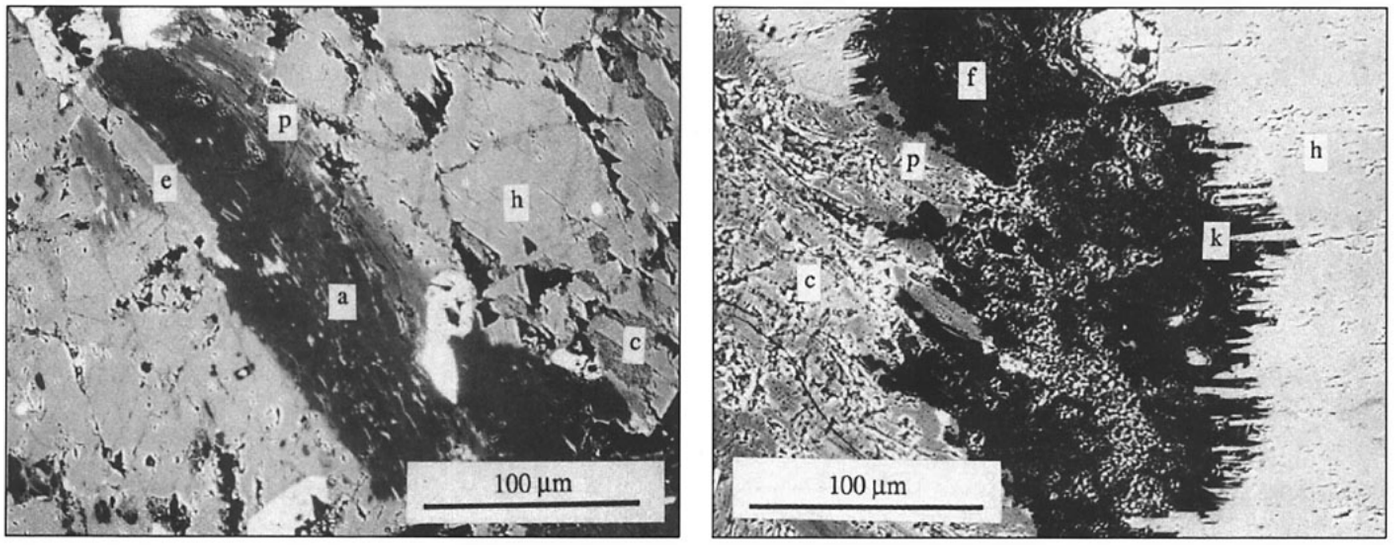

Figure 3. Back-scattered electron photomicrographs of amphibolite from the Feather River terrane. (A) Chlorite (c) in cracks in hornblende (h), and albite (a), epidote (e), and pumpellyite (p) replacing plagioclase; sample M126. (B) Hornblende crystal (h) overgrown by a 10-µm fringe of actinolite (k), and muscovite crystal (left side) replaced by pumpellyite (p) and chlorite (c) in sample M111; (f) K-feldspar. The long axes of the pumpellyite crystals parallel the mica cleavage.

blages are shown in Figure 4, and the latest mineral assemblage is albite + chlorite + actinolite + stilpnomelane + phengite + quartz + calcite + hematite(?). The mafic and sedimentary rocks are isofacial; the mafic blocks are not high-pressure blocks in a lower-pressure matrix.

Rocks of the Red Ant terrane are broken by east-dipping reverse faults, but the most characteristic structure is centimeter-scale ptygmatic folds that pervade layered lithologies (Schweickert and others, 1980). Metasedimentary rocks contain a well-developed phyllitic to schistose foliation parallel to compositional layering. The limbs and axial planes of early tight to isoclinal, rootless intrafolial folds parallel the foliation. These early folds, lineations, and the foliation predate the ptygmatic folds, which have dominantly northwest-striking axial planes and variably plunging axes (Figs. 5A, 5B). Similar structures do not occur in adjacent terranes. Quartz crystals deformed by a combination of dislocation creep, as indicated by undulatory extinction and subgrain formation, and dissolution and precipitation.

Several petrographic observations indicate that recrystallization both predated and accompanied ptygmatic folding and veining: (1) folia formed by mica, sodic amphibole, and lawsonite crystals are folded, and metamorphic phases in fold hinges are partially recrystallized; (2) epidote and lawsonite crystals are boudinaged; (3) there is a complete spectrum of early, strongly deformed veins to late, weakly deformed veins containing quartz, albite, chlorite, crossite, epidote, lawsonite, and phengite; (4) fibrous vein fillings (particularly sodic amphibole, phengite, and sphene) nucleated on wall minerals and recorded movements of the vein walls in their crystal shape. There is no indication that high-pressure phases grew after the ptygmatic folding.

Thus, textural relationships yield a chronology of events in the Red Ant terrane. The blueschist-facies metamorphism occurred prior to and during ptygmatic folding and vein formation. The pumpellyite-actinolite–facies metamorphism occurred after the blueschist-facies metamorphism, and the fibrous or radiating habits of stilpnomelane and some actinolite crystals indicate that they too postdate the folding.

Calaveras Terrane

The Calaveras terrane in the northern Sierra Nevada is a broken formation composed of phyllite, chert, and minor volcanic rocks (Hietanen, 1981; Hacker, 1984; Edelman and others, 1989b). It contains *in situ* chert with Late Triassic radiolarians (Irwin and others, 1978): rare carbonate olistoliths or fault blocks with Pennsylvanian-Permian, Early Permian, and Permo-Carboniferous to Early Triassic fossils (Hietanen, 1981; Standlee and Nestell, 1985). The study area contains only metasedimentary rocks—predominantly chert and quartzofeldspathic argillite bearing detrital hornblende, plagioclase, quartz, apatite, and zircon. Sedimentary layering in the Calaveras terrane is transposed to form a foliation that strikes north-northwest and dips steeply east (Fig. 5C). This pervasive foliation is locally crenulated on the scale of millimeters (Fig. 5D). Long axes of nematoblastic minerals parallel the foliation, indicating that the minerals grew prior to and/or during deformation. Regionally developed metamorphic mineral assemblages, such as actinolite + pumpellyite + muscovite + quartz + calcite + magnetite, are compatible with pumpellyite-actinolite facies metamorphism (Table 1). Folded and attenuated quartz veins in the Calaveras terrane are not as densely spaced or deformed as those in the Red Ant terrane, but they are more densely spaced and deformed than those in the Clipper Gap Formation.

Slate Creek Terrane

The Slate Creek terrane is a Late Triassic immature intraoceanic arc (Pb/U zircon ages of 202–209 Ma; Edelman and others, 1989a; Saleeby and others, 1989). Relict volcanic pyroxenes analyzed in this study support this interpretation and also suggest a contribution from a within-plate alkalic source (Fig. 6).

TABLE 1. METAMORPHIC MINERAL ASSEMBLAGES IN VOLCANIC AND VOLCANOGENIC ROCKS CONTAINING AT LEAST ONE Ca-Al SILICATE

Na-Am	Act	Ep	Pmp	Lws	Mu	Bio	Chl	Stlp	Ab	Mc	Qtz	Cc	Sph	FeO_x	FeS_x	Var	Assemblage	Samples
Clipper Gap Formation																		
	●				○	○	●		○	○	●		○	●	○	3	B–E	Y22, Y77, Y96, Y120, Y209, Y214, Y228
	●					●					●			●	●			Y30
		●			●				●		●							Y95
		●					●		●			●			●			Y80
		●				○			●	○	●		●	●				Y28, Y37, Y210
		●			●	○	●		○	○	●	○	○	●	○	3	A–E	Y27, Y34, Y117, Y208, Y211
	●	●						●	●		●		●					Y203
	●	●							●		●		●	●				Y122
	●	●					●		●	●	●	●	●			3	B or C	Y252a
	●	●				○	●		○	○	●	○	○	●	○	2	B1 or C1	Y7, Y65, Y93, Y94, Y109, Y113, Y123, Y206, Y212
		●	●			●			●	●	●		●	●	●	3	D1 or E1	Y215
Calaveras terrane																		
		●			●				●		●			●				Y87
		●			●		●		●		●	●						Y107, Y86, Y88
		●			●		●				●	●	●	●	●	3	A–E	M8A
			●		●		●		●		●		●	●	●	3	D or E	MB1
	●		●		●	●	●		●		●	●	●	●	●	2	D2 or E2	Y72
Slate Creek terrane																		
		●			●				●		●	●						Y16, Y48
		●			○	○	●		●		●	○			●			Y44, Y67, Y68, Y69, Y89, Y90, Y94, Y99
		●			●		●		●			●						Y70, Y98
	●	●			○		●		●	○		○	○	●	○			Y84, Y85, Y105
	●	●			●				●		●	●						Y52, Y53
	●	●			●		●		●		●	●				3	B or C	Y76
	●	●			○		●		●	○	●		●	●	●	2	B1 or C1	Y73, Mb3
	●		●				●	●	●		●		●	●		2	D2 or E2	M8C
	●		●				●		●				●	●	●			MB2
	●	●	●		●		●		●		●		●	●		1	B/C ↔ D/E	Y45, Y54, M8B
Red Ant terrane, pumpellyite-actinolite facies																		
		●			●		●	●	●		●		●	●		3	A–E	M21
		●		●			●		●		●		●	●		2		M6A
	●	●					●		●				●	●	●			M63
	●	●			●		●	●	●		●	●	●	●	●	2	B1 or C1	M76
	●		●		○	○	●		○	●	●		●	●	○	2	D2 or E2	M40b, M201
		●	●			●	●		●	●		●	●	●				M36
	●	●	●		●		●		●		●		●			2	B2 or C2	M100
	●		●	●	●	●	●	●	●	●	●	●	●	○	●	2	B3 or E3	M5E
Red Ant terrane, blueschist facies																		
●		●		●			●		●		●		●			2	A2	Schweickert and others (1980)
●		●			○		●	○	●		●		●		○	3	A	M77, M117
●		●			○		●	○	○		●	○	●	●		2	A1	M203, M204, M205, RR1
Feather River terrane																		
	●				○		●	○	○					●				M66, M7b, M124
	●						●	○	●		●			●		3	B–E	M20, M24
		●				○	●		○			○	○	●				M40A, M43b, M54
			●		●			●	●	●	●			●				M55
			●		○		●	○	●		●		○	●		3	D or E	M56, M5d, M110, M118
			●		○		●	○	●	○	●		○					M35, M112, M125
						●	●		●					●				M105
	●	●																
	●	●			○		●	○	○		●			●		2	B1 or C1	M37, M42b, M5b, M127
		●	●				●						●					M121
		●	●		●		●		○		●			●		2	D1 or E1	M5c, M126, M128
	●		●		○		●		●				○					M26, M101, M123
	●		●				●		●	●				●				M12
	●		●		○	○	●		●		●	○	○	●	○	2	D2 or E2	M39, M6b, Ma1, M119
	●	●	●						●									M6D
	●	●	●				●				●		●			2	B2 or C2	M28
	●	●	●				●		●					●				M43A
	●	●	●				●		●		●		●	●		1	B/C ↔ D/E	M27, M6E, M106, M111

Note: ●: present in all samples; ○: present in some samples. Na-Am: sodic amphibole; Act: actinolite; Ep: epidote; Pmp: pumpellyite; Lws: lawsonite; Mu: phengite; Bio: biotite; Chl: chlorite; Stlp: stilpnomelane; Ab: albite; Mc: microcline; Qtz: quartz; Cc: calcite; Sph: sphene; FeO_x: hematite or magnetite; FeS_x: pyrite, pyrrhotite, and chalcopyrite. Var: variance of quartz-saturated assemblages in the CaO-Fe_2O_3-$(Fe,Mg,Mn)O$-Al_2O_3 system, if less than 4. Assemblage: matches labels in Figures 13 and 14.

Volcanic rocks predominate in the study area; they include fine-grained layered tuff and flow rocks with a metamorphic foliation defined by compositional variation and by aligned plagioclase and amphibole porphyroclasts (Figs. 5E, 5F). The foliation is crenulated locally on the scale of millimeters. These crenulations are morphologically similar to, and contiguous with, structures in the underlying Calaveras terrane. Volcanic plagioclase crystals are replaced by phengite + albite + epidote + pumpellyite. Most hornblende and clinopyroxene crystals are replaced by actinolite + chlorite, others by epidote + pumpellyite (Fig. 7). Low-variance assemblages listed in Table 1 are compatible with pumpellyite-actinolite–facies metamorphism. Cracks within, and strain shadows adjacent to, plagioclase and hornblende porphyroclasts contain deformed actinolite, pumpellyite, chlorite, and quartz, indicating that the pumpellyite-actinolite facies metamorphism occurred during foliation development. Only some of the metamorphic minerals recrystallized during crenulation development, indicating that this late folding is syn- to post-metamorphic.

Clipper Gap Formation of the Fiddle Creek Terrane

The Fiddle Creek terrane is by far the most areally extensive unit in the Yuba River area. It includes three units, from bottom to top: (1) the Triassic or older Indian Creek ophiolitic mélange; (2) the Owl Gulch volcanics, intra-

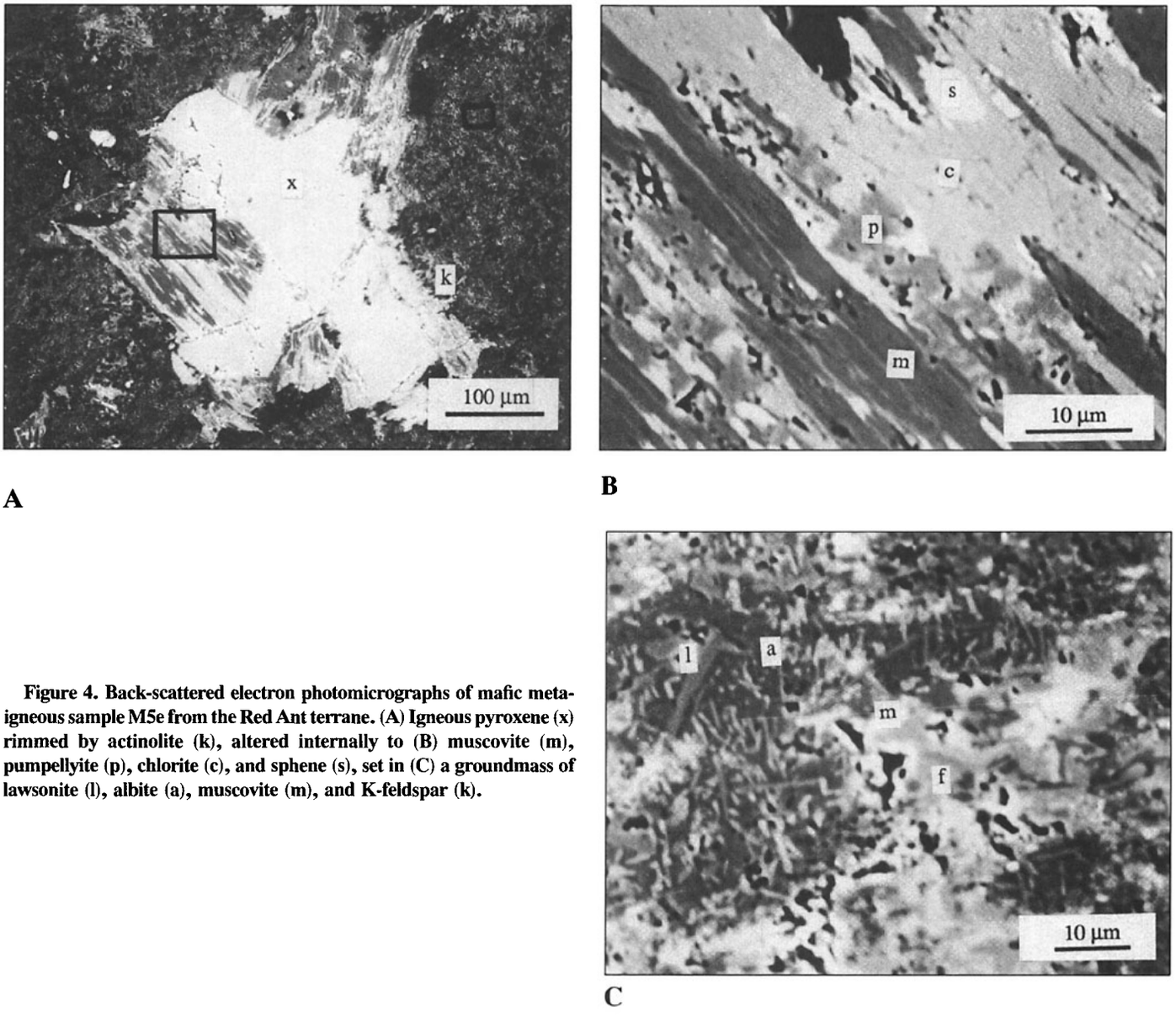

Figure 4. Back-scattered electron photomicrographs of mafic metaigneous sample M5e from the Red Ant terrane. (A) Igneous pyroxene (x) rimmed by actinolite (k), altered internally to (B) muscovite (m), pumpellyite (p), chlorite (c), and sphene (s), set in (C) a groundmass of lawsonite (l), albite (a), muscovite (m), and K-feldspar (k).

oceanic-arc rocks that overlie and intrude(?) the ophiolitic mélange; and (3) the Clipper Gap Formation, which is a Triassic-Jurassic broken formation and mélange deposited on the Owl Gulch (Dilek, 1989; Edelman and others, 1989b). Only the Clipper Gap Formation crops out in the study area. Generally weaker metamorphic recrystallization in this unit provides an opportunity to study the primary features of its sedimentary and volcanic components. Because the Clipper Gap Formation is the largest unit in the Yuba River area, this information is of considerable import for the tectonic history.

Primary Sedimentary and Volcanic Features. The Clipper Gap varies along strike from a broken formation along the North Yuba River to mixed broken formation and mélange on the South Yuba (Fig. 8). The broken formation is similar to type-II mélange of Cowan (1985), and the mélange is similar to Cowan's type-III mélange. The non-exotic component of the Clipper Gap includes rocks grading from radiolarian chert to tuff, pillow lava, and volcanogenic and quartzose clastic rocks. These rocks are all interbedded in continuous sequences, and disrupted sections are composed primarily of these rock types as well. Rocks vary from relatively undeformed where bedding is preserved and lithologies are slightly intermixed, to strongly deformed where bedding is no longer discernible and exotic rock types are juxtaposed. Successive stages of disruption can be seen in nearby outcrops. First, more competent layers of sandstone or volcanic rock fractured, and the fractures were filled either with argillite injected from adjacent beds or with quartz dissolved locally or nearby (Fig. 8A). Then the fractured pieces separated and were mixed in the argillite (Fig. 8B). Large strains are manifested by transposed bedding and folding. The strongest mixing is evident in mélange where blocks of markedly different lithologies are intimately associated, and all traces of depositional layering are obliterated (Fig. 8C).

Exotic blocks are pebble to house sized, and they include ultramafic rock, gabbro, basalt, limestone, epidote amphibolite, quartzofeldspathic schist, recrystallized chert, and crenulated quartz-mica schist. Amphibolite blocks contain tschermakitic hornblende + epidote + andesine + almandine + rutile, and

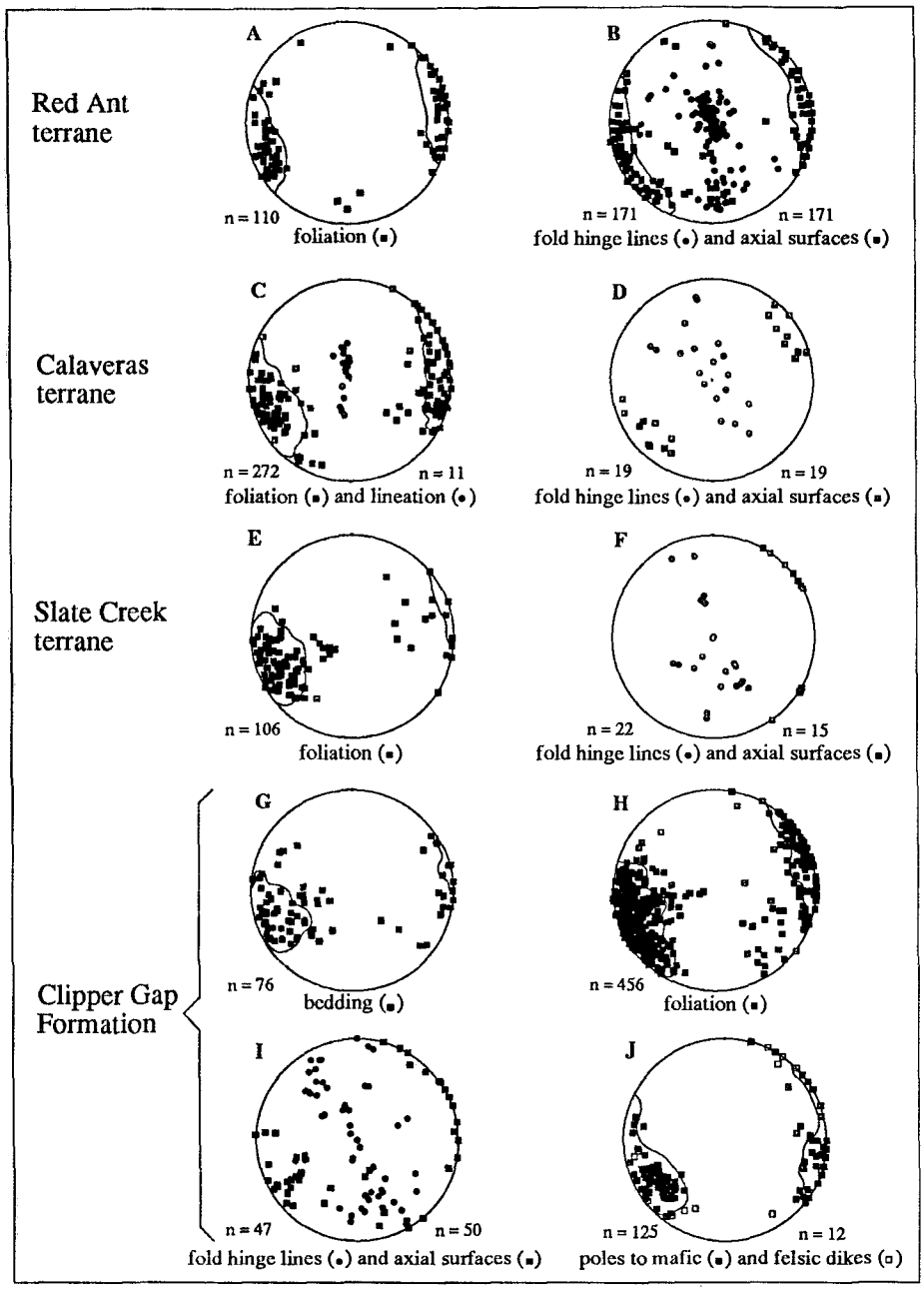

Figure 5. Equal-area stereographic projections of structures in the Yuba River area. Contours enclose densities that exceed the mean by 3 standard deviations. Red Ant terrane: (A) foliation, (B) ptygmatic folds in metasedimentary rock. Calaveras terrane: (C) foliation and lineation, (D) crenulations of foliation. Slate Creek terrane: (E) foliation, (F) crenulations of foliation. Clipper Gap Formation: (G) bedding, (H) foliation, (I) folds of bedding, (J) mafic dikes and felsic dikes from the Yuba Rivers pluton.

quartz-mica schist blocks contain helicitic almandine + muscovite + biotite + microcline + porphyroblastic albite + quartz. All are retrogressed to greenschist-facies minerals including chlorite, muscovite, stilpnomelane, and sphene. This retrogression may have accompanied low-grade recrystallization of the mélange matrix.

Much of the Clipper Gap contains few if any exotic blocks and is instead chiefly disrupted argillite, volcanogenic rocks, and chert containing Middle Triassic and Late Triassic–Early Jurassic radiolaria (Irwin and others, 1978; Hietanen, 1981). The dominant rock type is arkosic, subfeldspathic-lithic, and volcanic-lithic argillite or tuff. Detrital grains include quartz with topotactic cement overgrowths, An_{00-33} plagioclase, actinolite-tschermakite, salite-augite, muscovite, biotite, sphene, apatite, ilmenite, pyrite, zircon, spinel, and radiolarians.

Rare, centimeter- to decimeter-thick, massive to weakly laminated, quartzose sandstone and conglomerate beds are interbedded and gradational with argillite. They contain detrital metamorphic quartz, plagioclase, and actinolite grains, as well as clasts of deformed radiolarian chert and argillite, microgabbro, marble, calcarenite, and greenschist-facies sedimentary and mafic schists. Delicate ball-and-pillow and flame structures are locally preserved.

Volcanogenic conglomerate and sandstone are more abundant than quartzose clastic rocks, comprising clasts of pumice, clinopyroxene basalt, granodiorite, clinopyroxenite, gabbro, limestone, chert, mafic and sedimentary schist, grains of salite-augite rimmed by hornblende, angular andesine-labradorite with quenched liquid inclusions, alkali feldspar, magnesiohastingsite, and calcite. They also grade with decreasing grain size into argillite. Pyroxene (Fig. 6), and bulk-rock (Hietanen, 1981) compositions indicate that the rocks were derived from a volcanic arc.

All of the detrital rocks were clearly derived from sources including a mafic volcanoplutonic arc and metamorphosed and unmetamorphosed mafic and quartzofeldspathic rocks. Some detritus was probably derived from intraformational sources. A potential nearby source for the salite and tschermakite is the amphibolite-facies rocks of the Feather River terrane (Hacker and Peacock, 1990); geochronologic data supporting this suggestion are presented below. Detrital-quartz grains with cement overgrowths may have come from the feebly metamorphosed quartz arenites in the Shoo Fly Complex (Hietanen, 1981). The provenance of volcanogenic rocks may have been volcanoplutonic arc rocks of the Northern Sierra terrane or more proximal westerly magmatic rocks such as those of the Smartville terrane.

Microgabbro to quartz monzogabbro dikes and locally pillowed flow rocks account for a moderate part of the Clipper Gap unit. They contain multiply zoned, broken and swallow-tail euhedral oligoclase, euhedral ferrohornblende, quartz, alkali feldspar, and diopside-augite partially replaced by amphibole. The dikes cut across veins and foliation in the clastic rocks (Fig. 5J), suggesting that they intruded late in the deformation history.

Metamorphism and Deformation. Metasedimentary rocks in the Clipper Gap Formation

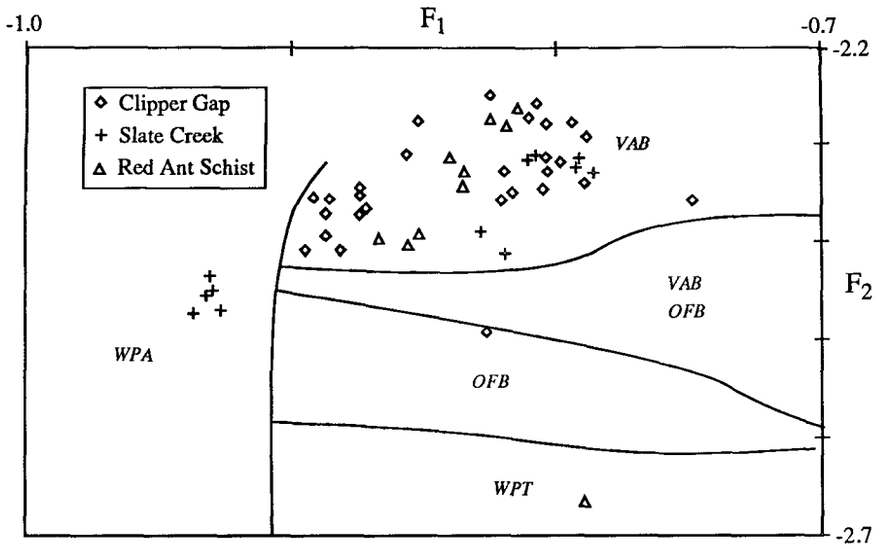

Figure 6. Discriminant diagram of Nisbet and Pearce (1977), illustrating that most volcanic pyroxenes from the Yuba River area were probably derived from an arc, although some may have been erupted from within-plate sources. VAB: intraoceanic arc basalt, OFB: mid-ocean ridge basalt, WPA and WPT: within-plate basalts. $F_1 = -0.012\ SiO_2 - 0.0807\ TiO_2 + 0.0026\ Al_2O_3 - 0.0012\ FeO^* - 0.0026\ MnO + 0.0087\ MgO - 0.0128\ CaO - 0.0419\ Na_2O$. $F_2 = -0.0469\ SiO_2 - 0.0818\ TiO_2 - 0.0212\ Al_2O_3 - 0.0041\ FeO^* - 0.1435\ MnO - 0.0029\ MgO + 0.0085\ CaO + 0.0160\ Na_2O$. This technique is ~70% likely to identify the correct magma type, according to Nisbet and Pearce.

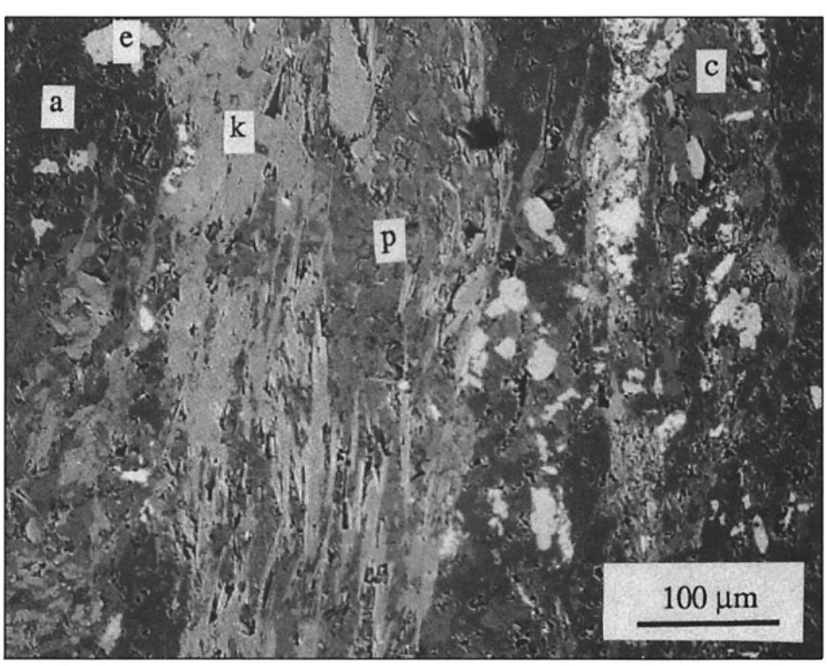

Figure 7. Back-scattered electron photomicrograph of volcanic sample M8b from the Slate Creek terrane, showing intergrown pumpellyite (p), actinolite (k), epidote (e), chlorite (c), and albite (a).

lack diagnostic metamorphic mineral assemblages—some contain metamorphic quartz, phengite, biotite, pumpellyite, and/or microcline, but detrital pyroxene, amphibole, and plagioclase are widespread. Dikes and flow rocks commonly contain igneous clinopyroxene, hornblende, and plagioclase partially altered to actinolite, epidote, albite, and sphene (Table 1). Actinolite and epidote are widespread in volcanic rocks, but other metamorphic minerals are uncommon.

Foliation is formed by transposed bedding and laminae of opaque minerals and phyllosilicates. Bedding and foliation are subparallel, striking 130°–190° and dipping 70°E to 85°W (Figs. 5G, 5H). The only lineation is formed by bedding-cleavage intersections. Argillite contains anastomosing cataclastic zones rich in opaque minerals (web structure of Byrne, 1984). Seams of opaque minerals and phyllosilicates form a rough disjunctive cleavage in argillite and limestone (Fig. 9). Truncations of crystals and veins at these surfaces and shortening of veins orthogonal to these surfaces indicate that the cleavage and veins formed by stress solution and redeposition. Thick chert beds were unable to deform solely by solution-transfer creep, and they contain brecciated fragments connected by syntaxial quartz fibers.

Overturned geopetal structures and local fold hinges indicate pervasive isoclinal folding of the bedding. Most folds are harmonic, with rounded to angular closures, and moderate to tight interlimb angles. Fold wavelengths and amplitudes vary from centimeters to meters, and their axial surfaces are subparallel to foliation. Hinge lines plunge at variable angles to the northwest and southeast in the foliation (Fig. 5I). Cores of folds are commonly broken by faults formed along axial-planar cleavage surfaces, and fold limbs are boudinaged and transposed.

The broken formation and mélange are inferred to have formed primarily by tectonic disruption of initially interbedded rocks because (1) the disrupted rocks are not overlain or laterally bounded by coherent sedimentary strata, (2) folds are not truncated by depositional contacts, (3) cataclastic web structures are present, (4) there are no clastic dikes, (5) stress solution occurred during folding and faulting, and (6) veins suggest fluid pressures and confining pressures higher than expected during mass wasting. Not all of the disruption need be the result of tectonism, however—many of the clastic rocks may be debris flows.

The structurally lowest part of the Clipper Gap Formation exposed on the North Yuba River (Fig. 14 of Edelman and others, 1989b), just above the depositional contact with the

A

B

C

Figure 8. Sequential photographs illustrating how progressive disruption produced broken formation and mélange in the Clipper Gap Formation along the South Yuba River.

(A) Volcanogenic turbidites extended subparallel to bedding by a combination of small-scale normal faulting and quartz dissolution and reprecipitation.

(B) Disrupted quartzose sandstone beds in argillite matrix; quartzose veins are transposed parallel to the foliation and are difficult to see.

(C) Clasts of volcanic rock (background), veined argillite (foreground), chert, limestone, and quartzose sandstone (center) in a matrix of volcanogenic argillite. Pen for scale.

Lower Jurassic(?) Owl Gulch volcanics, contains key information about the evolution of the Formation. There the Clipper Gap is not a broken formation or mélange, and it is much less deformed than are higher portions of the unit. It is composed of massive to bedded argillite overlying carbonate-matrix debris flows, the latter containing blocks of lava, volcaniclastic fragments, and thick-bedded gray chert. Thus, the lowest part of the Clipper Gap represents Lower Jurassic mass-wasting deposits overlain by pelagic sediments.

New $^{40}Ar/^{39}Ar$ Ages

Four new $^{40}Ar/^{39}Ar$ ages were obtained (Figs. 2A, 10; Table 2). Hornblende was analyzed from sample Y227, a volcanic boulder from a proximal lahar within the Clipper Gap Formation at Edwards Crossing on the South Yuba River. The lahar is composed of volcanic and plutonic clasts to 40 cm in diameter with minor chert and sandy limestone clasts in a matrix that grades from plagioclase-rich sandstone to argillite. Pyroxenite and aphanitic vesicular volcanic cobbles occur as rare clasts. The lahar is intruded by the mafic dikes that are common throughout the Formation and is cut locally by deformed zones. The dated sample consists of 50% igneous plagioclase and 15% igneous hornblende in a fine-grained mesostasis of metamorphic albite + biotite + magnetite + quartz + sphene. The hornblende crystals are broken but not altered. Plagioclase crystals have multiple oscillatory zoning and mechanically induced twins, suggesting residence in a magma chamber followed by deformation during

eruption. The age spectrum may indicate partial argon loss on the order of 10%. The high-temperature steps, 1070–1400 °C, yield an inverse isochron age of 174.3 ± 1.9 Ma, whereas steps at lower temperatures were fitted by an inverse isochron of 165.1 ± 2.6 Ma. This provides multiple useful age constraints: the age of the arc provenance is 174 Ma; lahar deposition, metamorphism, deformation, and intrusion by dikes all postdate 174 Ma. The low-temperature steps may reflect a reheating event at ca. 165 Ma, perhaps related to intrusion of the nearby 159-m.y.-old Yuba Rivers pluton (Pb/U, Edelman and others, 1989a; Saleeby and others, 1989).

Igneous hornblende was analyzed from Y213, a sample from a pluton that cuts foliated Clipper Gap and Slate Creek terrane rocks at the confluence of Bloody Run and the Middle Yuba River. The pluton also underwent subsolidus deformation, but not to the same degree as the host rock. The sample consists of 70% plagioclase, 15% hornblende, and 15% microcline. The hornblende crystals are cracked but unaltered, whereas plagioclase is extensively altered to muscovite, and trace amounts of sphene and chlorite are present. These minerals are compatible with pumpellyite-actinolite–facies metamorphism, and it is possible that the pluton and country rock were metamorphosed together. Excluding disturbed low-temperatures steps, an isochron age of 164.8 ± 0.5 Ma is considered to be the minimum crystallization age and maximum metamorphic age of the pluton. Note that this age coincides with the reheating event inferred for sample Y227. This datum constrains the end of movement on the Gillis Hill fault and indicates that substantial deformation of the Clipper Gap and Slate Creek units predated 165 Ma. Deformation of the pluton implies that some deformation of the country rock is either syn- or post–165 Ma.

M111 is an amphibolite-facies mafic rock from the Feather River terrane which contains veins of pumpellyite and actinolite. An Ar/Ar step heating experiment was performed on a hornblende separate in the hope that low-temperature steps might reveal an indication of the age of the pumpellyite-actinolite–facies metamorphism. An inverse isochron of 343.7 ± 0.6 Ma can be fitted to the 1125–1400 °C steps. This represents the time for cooling through lower-amphibolite–facies temperatures, and coincides with 322 ± 27 Ma and 345 ± 9 Ma K/Ar ages on amphibolite obtained by Böhlke and McKee (1984). There is no indication of more recent Ar loss, demonstrating that temperatures remained well below 450 °C since Devonian time.

Y232 is a metasedimentary amphibolite-facies exotic block from the Clipper Gap Formation along the South Yuba River. It consists of 55% quartz, 25% muscovite, 10% biotite, 5% microcline, and 5% garnet. The muscovite crystals contain 3.1–3.3 Si atoms per formula unit, and the microcline crystals are lightly sericitized. The garnets have the composition $alm_{74-81}grs_{10-16}pyr_{08-10}spe_{01-02}$, inclusion trails, and strain shadows filled with chlorite. The biotite appears unaltered and has the composition $(K_{0.93}Na_{0.02})(Mg_{1.1}Fe_{1.3}Ti_{0.1}Al_{0.5})(Al_{1.2}Si_{2.8})O_{10}(OH)_2$. The Ar isotopic ratios for biotite from this sample are disturbed and yield a total fusion age of 282 Ma. The age spectrum for this sample is compatible with ~20% outgassing (McDougall and Harrison, 1988) from an initial age of ~350 Ma. The total fusion age is similar to a 273 ± 5 Ma K/Ar age reported by Böhlke and McKee (1984) for muscovite from the Feather River terrane, and the inferred initial age is similar to amphibolite M111 from the Feather River terrane. Thus, the source of this block is probably the Feather River terrane.

MINERAL CHEMISTRY

Information about physical conditions during the blueschist- and pumpellyite-actinolite–facies metamorphism can be obtained from mineral compositions. Calcic amphiboles in all units in the Yuba River area range from tremolite to actinolitic hornblende (Table 3). Tschermakitic compositions are notably absent, implying that amphibolite-facies conditions were never realized. Sodic and sodic-calcic amphiboles in the Red Ant terrane include magnesioriebeckite, crossite, ferroglaucophane, and winchite (Hacker and Goodge, 1990).

Potassium–white mica is abundant in all units except for the Clipper Gap Formation, where it occurs locally. Only K–white mica

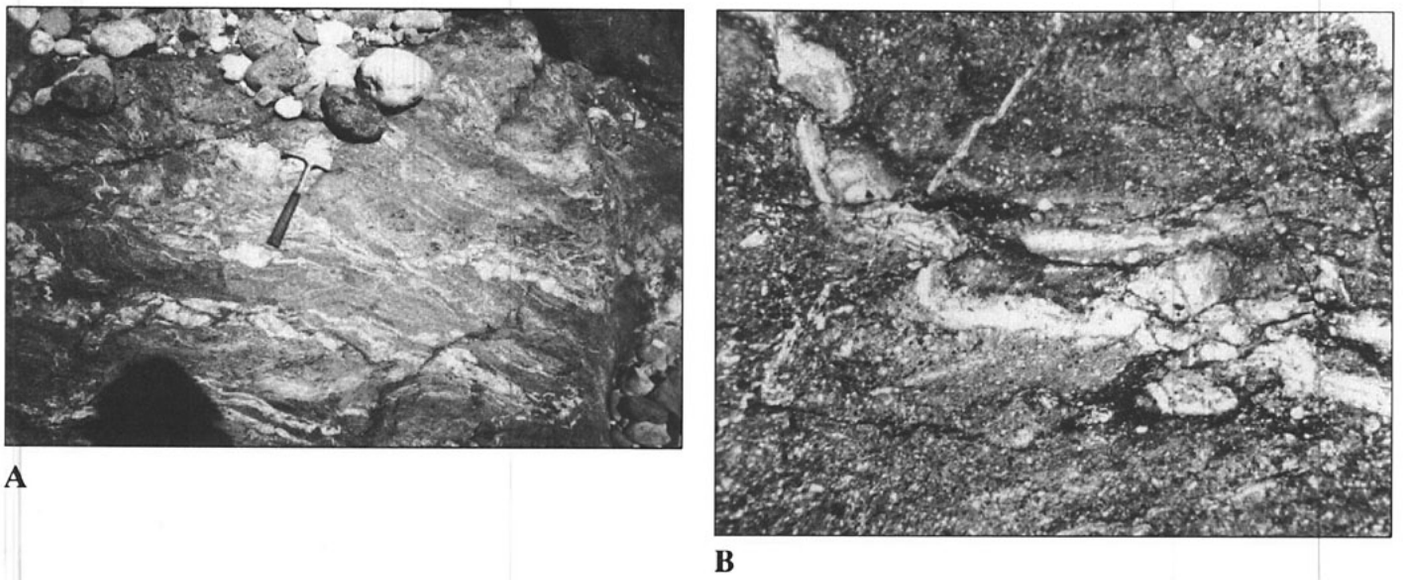

Figure 9. Quartz veins in the Clipper Gap unit. (A) Argillite outcrop with ~20 vol% quartz veins that have been transposed parallel to the foliation. (B) Thin section of sample Y215 illustrating opaque mineral seams and quartz veins being redissolved; field of view is 0.5 mm.

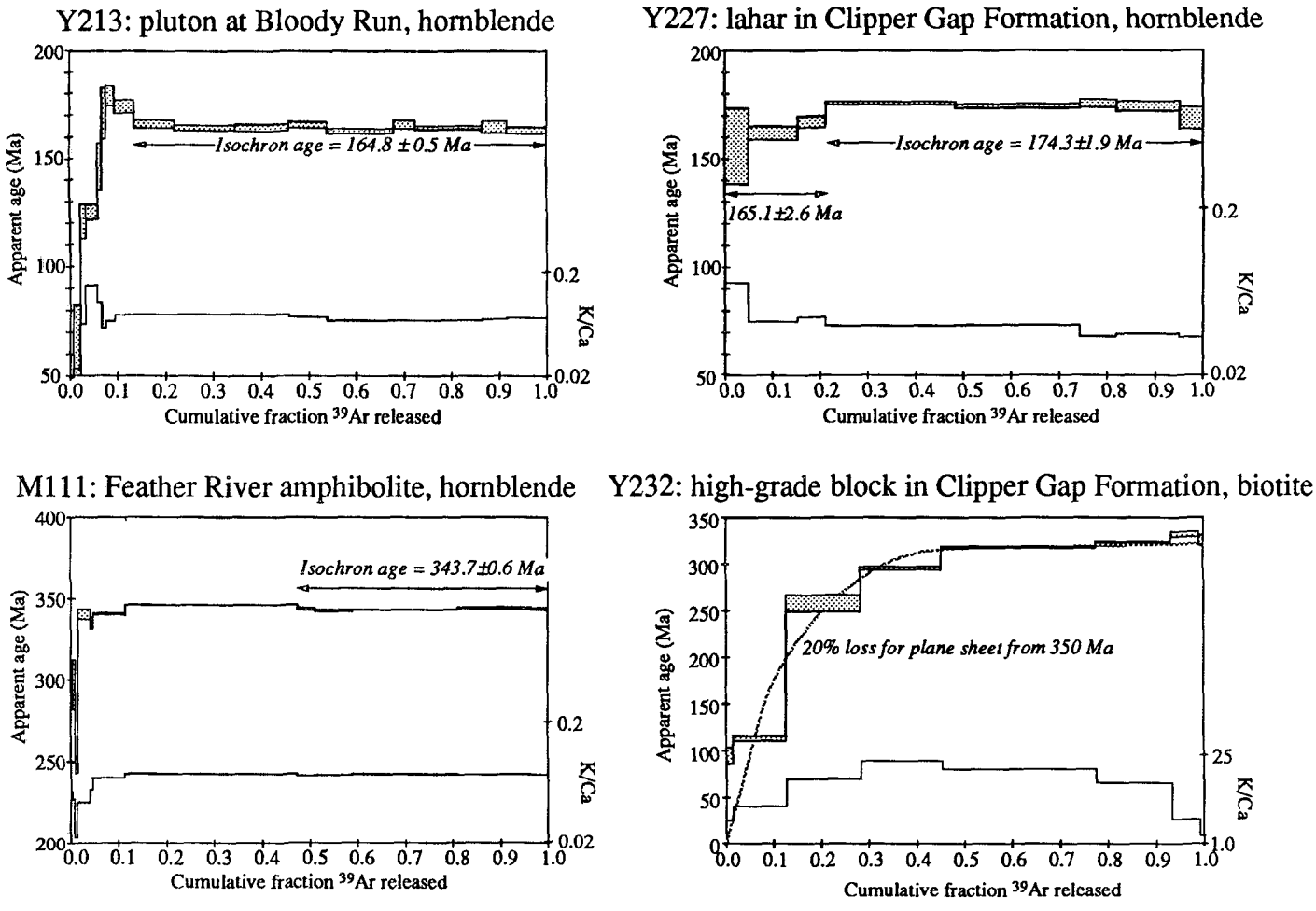

Figure 10. Age spectra and K/Ca ratios for samples dated by Ar/Ar method. One-sigma uncertainties are shown. K/Ca scale is logarithmic.

has been found—paragonite or margarite were not found, although Guidotti and others (1979) reported coexisting white-mica trios south of the study area. The phengite crystals show phengite substitution, $(Fe^{2+},Mg,Mn)Si(Al^{VI},Fe^{3+},Ti)_{-1}Al_{-1}$, of 0.2–0.7 per formula unit (pfu) (Table 3), comparable to phengite from other high-pressure terranes (Evans and Patrick, 1987). The maximum number of Si atoms pfu in phengite shows a progressive increase eastward from one unit to the next (Fig. 11), compatible with an eastward increase in pressure. Muscovite Si content does not depend on the presence or absence of iron oxide, biotite, quartz, or microcline, and is instead quite variable. Indeed, different phengite crystals within individual samples display the same degree of variation as that exhibited by all phengite crystals within a given unit. Such variation is attributable to incomplete recrystallization of detrital crystals.

Biotite occurs sporadically throughout the Yuba River area, except in blueschist-facies rocks of the Red Ant terrane. It ranges in composition from $K_{0.9}(Mg_{1.19}Mn_{0.02}Fe^{2+}_{0.14}Fe^{3+}_{0.00}Ti_{0.17}Al_{0.21})(Al_{1.39}Si_{2.61})O_{10}(OH)_2$ to $K_{0.9}(Mg_{1.94}Mn_{0.02}Fe^{2+}_{0.08}Fe^{3+}_{0.46}Ti_{0.05}Al_{0.45})(Al_{1.16}Si_{2.84})O_{10}(OH)_2$, and there is no systematic variation regionally.

Chlorite is abundant in all units except for the Clipper Gap Formation, where it occurs locally. There is no systematic regional variation in chlorite composition, and the variation in the composition of chlorite crystals in a single outcrop is comparable to the variation in composition within a single unit (Table 3). Much of the variation can be accounted for by substitution of $(Mg,Fe^{2+})Si$ for $Al^{VI}Al^{IV}$, producing variations of 1.05–1.45 pfu. There is no correlation between chlorite MgO content and the minerals with which it coexists, unlike that reported by Aiba (1982) for pumpellyite-actinolite schists of the Chichibu belt in Japan.

Stilpnomelane is found predominantly in the Feather River and Red Ant terranes (Table 4); analyses were normalized to 8 Si atoms pfu, after Brown (1971). Compositions range from $(K,Ca)_{0.3}Mg_{2.1}Mn_{0.4}Fe_{3.3}Al_{1.1}Si_8O_{27}(OH)_4$ to $(K,Ca)_{0.2}Mg_{1.6}Mn_{0.1}Fe_{3.9}Al_{1.2}Si_8O_{27}(OH)_4$; analyses rich in Al_2O_3 and FeO are impoverished in MnO and MgO, and vice versa.

Epidote is a widespread mineral in all units, and contains 8–33 mol% pistacite, $Fe^{3+}/(Fe^{3+}+Al)$ (Table 3). Unzoned epidotes have ≥20 mol% pistacite, and zoned epidotes typically have Fe-rich cores and Fe-poor rims. Coexisting pairs of epidote minerals—as reported by Hietanen (1974) for contact aureoles north of the study area—were not recognized. No correlation between epidote composition and the minerals with which it coexists was observed, unlike that reported by Nakajima (1982) for pumpellyite-actinolite schists of the Sanbagawa belt of Japan.

Pumpellyite is found in all units in the Yuba River area. In this study, analyses were nor-

TABLE 2. Ar/Ar DATA

Hornblende from mafic amphibolite of Feather River terrane

Sample M111		J = 0.01089257		wt = 13.9 mg			400–600 μm grain size	
T(°C)	$^{40}Ar(v)$	$^{40}Ar^*/^{39}Ar^K$	$^{37}Ar/^{39}Ar$	$^{36}Ar/^{39}Ar$	K/Ca	$\Sigma\ ^{39}Ar$	$^{40}Ar^*$	Age (Ma) ± 1 σ
600	1.0038	3.7839	8.4559	0.1490	0.06	0.003	0.066	73 ± 23
700	9.9325	−5.8307	8.0422	4.1242	0.06	0.004	−0.005	−118 ± 704
800	1.9885	16.4520	9.0156	0.1349	0.05	0.009	0.282	297 ± 15
900	0.9385	13.5230	16.1954	0.0389	0.03	0.015	0.513	247.9 ± 5.3
1000	4.4769	19.0740	9.5307	0.0221	0.05	0.041	0.736	340.5 ± 3.1
1030	0.9689	18.8043	7.8006	0.0201	0.06	0.046	0.753	336.1 ± 3.4
1070	9.2908	19.0783	6.5157	0.0037	0.07	0.114	0.944	340.6 ± 0.6
1100	50.2958	19.4477	6.1193	0.0034	0.08	0.473	0.950	346.6 ± 0.5
1125	5.3805	19.2983	6.2579	0.0037	0.08	0.511	0.944	344.2 ± 0.7
1160	10.5765	19.2189	6.2172	0.0030	0.08	0.588	0.954	342.9 ± 0.6
1200	30.8251	19.2608	6.1197	0.0034	0.08	0.811	0.949	343.6 ± 0.6
1230	7.3114	19.3418	6.1537	0.0032	0.08	0.863	0.951	344.9 ± 0.5
1270	5.4113	19.3023	6.1781	0.0037	0.08	0.902	0.945	344.2 ± 0.7
1330	8.7311	19.3077	6.1311	0.0045	0.08	0.964	0.934	344.3 ± 0.8
1400	4.9972	19.2762	6.1460	0.0028	0.08	1.000	0.958	343.8 ± 0.6

Isochron age = 343.7 ± 0.6 Ma (1125–1400 °C; MSWD = 0.01)
Total fusion age = 342.3 ± 0.7 Ma
Weighted mean plateau age = 343.7 ± 0.3 Ma (1125–1400 °C; 53% of total ^{39}Ar)

Hornblende from lahar in Clipper Gap Formation

Sample Y227		J = 0.0110487		wt = 4.2 mg			200–400 μm grain size	
T(°C)	$^{40}Ar(v)$	$^{40}Ar^*/^{39}Ar^K$	$^{37}Ar/^{39}Ar$	$^{36}Ar/^{39}Ar$	K/Ca	$\Sigma\ ^{39}Ar$	$^{40}Ar^*$	Age (Ma) ± 1 σ
900	11.5282	8.1648	6.6171	0.3150	0.07	0.050	0.076	155.8 ± 18
1000	2.8234	8.5182	10.6673	0.0148	0.05	0.153	0.636	162.3 ± 3.1
1030	1.4756	8.7921	10.1057	0.0101	0.05	0.212	0.727	167.3 ± 2.0
1070	6.3540	9.3036	11.2567	0.0066	0.04	0.481	0.811	176.5 ± 0.0
1100	5.8684	9.2229	11.1178	0.0052	0.04	0.743	0.845	175.1 ± 0.0
1150	1.8470	9.3097	12.8014	0.0079	0.04	0.819	0.780	176.6 ± 1.6
1260	3.2081	9.0496	12.4606	0.0090	0.04	0.951	0.750	171.9 ± 2.0
1400	1.2540	8.8784	12.9249	0.0113	0.04	1.000	0.699	168.8 ± 4.9

Isochron age = 165.1 ± 2.6 Ma (900–1030 °C; MSWD = 1.4)
Isochron age = 174.3 ± 1.9 Ma (1070–1400 °C; MSWD = 0.1)
Total fusion age = 171.8 ± 1.1 Ma
Weighted mean plateau age (1070–1400 °C; 79% of total ^{39}Ar) = 174.8 ± 0.6 Ma

Hornblende from pluton at Bloody Run

Sample Y213		J = 0.0109361		wt = 4.1 mg			150–200 μm grain size	
T(°C)	$^{40}Ar(v)$	$^{40}Ar^*/^{39}Ar^K$	$^{37}Ar/^{39}Ar$	$^{36}Ar/^{39}Ar$	K/Ca	$\Sigma\ ^{39}Ar$	$^{40}Ar^*$	Age (Ma) ± 1 σ
600	0.3821	2.0147	16.4928	0.0495	0.03	0.007	0.045	39 ± 24
700	3.3555	2.9411	14.2745	0.2419	0.03	0.021	0.024	57 ± 26
800	0.7654	6.3530	6.7011	0.0377	0.07	0.034	0.343	121.2 ± 7.9
900	0.7053	6.6178	3.4942	0.0071	0.14	0.058	0.752	126.1 ± 3.4
950	0.2956	7.7321	4.7201	0.0101	0.10	0.067	0.711	146.4 ± 11
980	0.3460	9.1344	7.1344	0.0093	0.07	0.076	0.756	171.8 ± 12
1010	0.7072	9.5062	6.3757	0.0066	0.08	0.094	0.822	178.4 ± 4.6
1030	1.3006	9.3211	5.7512	0.0026	0.09	0.134	0.919	175.1 ± 3.2
1050	2.6476	8.8421	5.6711	0.0020	0.09	0.220	0.935	166.5 ± 1.6
1065	3.8397	8.6909	5.6862	0.0021	0.09	0.347	0.931	163.8 ± 1.2
1080	3.3735	8.7848	5.7093	0.0016	0.09	0.459	0.945	165.5 ± 1.7
1105	2.4157	8.6986	5.9504	0.0020	0.08	0.540	0.934	163.9 ± 1.4
1145	4.1750	8.7105	6.3060	0.0020	0.08	0.678	0.932	164.1 ± 1.0
1175	1.3501	8.8127	6.2578	0.0015	0.08	0.723	0.951	166.0 ± 1.8
1225	4.2573	8.7416	6.2723	0.0019	0.08	0.865	0.935	164.7 ± 0.9
1275	1.5511	8.7667	6.1297	0.0020	0.08	0.916	0.933	165.2 ± 2.7
1400	2.7437	8.6748	6.0183	0.0046	0.08	1.000	0.856	163.5 ± 1.5

Isochron age = 164.8 ± 0.5 Ma (1050–1400 °C; MSWD = 15)
Total fusion age = 161.3 ± 0.6 Ma
Weighted mean plateau age = 164.6 ± 0.5 Ma (1050–1400 °C; 87% of total ^{39}Ar)

Biotite from amphibolite-facies block in the Clipper Gap Formation

Sample Y232		J = 0.0052508		wt = 2 mg			100–200 μm grain size	
T(°C)	$^{40}Ar(v)$	$^{40}Ar^*/^{39}Ar^K$	$^{37}Ar/^{39}Ar$	$^{36}Ar/^{39}Ar$	K/Ca	$\Sigma\ ^{39}Ar$	$^{40}Ar^*$	Age (Ma) ± 1 σ
600	0.1632	10.2240	0.1696	0.0513	2.9	0.013	0.403	94.3 ± 8.6
700	1.2557	12.3083	0.1065	0.0368	4.6	0.126	0.531	113.0 ± 2.7
800	4.9457	29.3732	0.0425	0.1244	11	0.282	0.444	258.8 ± 9.1
900	3.2786	33.9190	0.0239	0.0214	20	0.452	0.843	295.7 ± 1.9
1000	6.2004	36.7707	0.0312	0.0107	16	0.775	0.921	318.6 ± 1.0
1050	2.9313	37.3827	0.0491	0.0049	10	0.933	0.963	323.3 ± 0.8
1100	1.2795	38.6146	0.1634	0.0250	3.0	0.991	0.839	333.0 ± 2.6
1200	0.2066	37.5614	0.2954	0.0317	1.7	1.000	0.800	324.7 ± 5.7

Total fusion age = 282 ± 1.6 Ma

Note: T: temperature; $^{40}Ar(v)$: measured volts of ^{40}Ar corrected for blank and reactor-produced ^{40}Ar; $^{40}Ar^*/^{39}Ar^K$: ratio of radiogenic ^{40}Ar to ^{39}Ar produced by irradiation of ^{40}K; $^{37}Ar/^{39}Ar$: ratio of corrected ^{37}Ar and ^{39}Ar; $^{36}Ar/^{39}Ar$: ratio of corrected ^{36}Ar and ^{39}Ar; K/Ca: inferred K/Ca ratio; $\Sigma\ ^{39}Ar$: cumulative ^{39}Ar released; $^{40}Ar^*$: radiogenic fraction of ^{40}Ar. MSWD: mean sum of weighted deviates; expresses the goodness of fit of the isochron and has an expected value of ~2.5 (Roddick, 1978).

malized to 24.5 oxygen atoms pfu (after Yoshiasa and Matsumoto, 1985). Assuming that all Fe is ferrous, normalization to 24.5 oxygen atoms yielded a slight excess of Si atoms pfu (6.05–6.17), nearly correct M2 site occupancy, $Al^{IV}+Fe^{2+}+Mg$ (1.86–2.07 pfu), and a deficiency in Na+Ca+Mn atoms pfu (3.74–3.96) (Table 3). Alternatively, assuming that all Fe is ferric, this normalization scheme yielded a smaller excess of Si atoms pfu (6.01–6.12), nearly correct M2 site occupancy (1.89–2.10 pfu), but a greater deficiency in Na+Ca+Mn atoms (3.73–3.93). Liou (1979), Nakajima (1982), Ishizuka (1985), and Springer and others (1992) also reported Ca+Na+Mn deficiencies in pumpellyite crystals normalized to 24.5 oxygen atoms. Recalculations based on fixed cation charge or number of cations also yield insufficient Ca+Na+Mn cations. This suggests that the Ca site in pumpellyite may contain ≈5–15 mol% vacancies or elements not analyzed.

All pumpellyites in the Yuba River area are aluminous (enough Al is present to fill the M1 sites). Most are compositionally similar to pumpellyite from pumpellyite-actinolite–facies rocks worldwide and dissimilar to pumpellyite from zeolite- and prehnite-pumpellyite–facies rocks (Passaglia and Gottardi, 1973; Zen, 1974; Coombs and others, 1976; Liou, 1979; Mevel, 1981; Brown and Ghent, 1983; Schiffman and Liou, 1983; Yoshiasa and Matsumoto, 1985). The pumpellyites contain as much as 4% MgO and 7% FeO*; two crystals contain as little as 1.2 and 1.4 wt% FeO*—less iron than has previously been reported for any natural pumpellyite. The pumpellyite crystal compositions do not show marked systematic regional variation.

Metamorphic albite containing up to 3 mol% anorthite was found in all units. Single crystals of oligoclase were not observed, nor were albite + oligoclase pairs. Original detrital and igneous plagioclase compositions from albite to anorthite persist as cores to albite crystals in all units.

Microcline is present in all units except the Calaveras terrane. None of the carbonate samples tested by X-ray diffraction contains aragonite, and zeolites and sodic pyroxenes are also absent. Sphene, magnetite, and hematite occur in all units.

DISCUSSION

Metamorphic Assemblages, Isograds, and Reactions

The epidote + actinolite + pumpellyite assemblage developed in the Yuba River area matches the pumpellyite-actinolite facies zone of the Haast Schist terrane, New Zealand (Kawachi, 1975), the Taveyanne Formation, Switzerland (Coombs and others, 1976), and the Sanbagawa and Chichibu Belts of Japan (Aiba, 1982; Nakajima, 1982). The blueschists in the Red Ant terrane contain epidote + sodic amphibole + hematite + chlorite + albite + quartz, and lack sodic

TABLE 3. ANALYSES OF COEXISTING MINERALS

Clipper Gap Formation, sample Y96				Calaveras terrane, sample Y72				Slate Creek terrane, sample M8b				
Mineral	Act	Mu	Bio	Act	Mu	Bio	Pmp	Act	Mu	Chl	Ep	Pmp
SiO_2	52.81	41.44	36.22	52.05	47.63	36.57	37.57	53.71	48.78	29.67	38.12	38.1
Al_2O_3	3.98	12.57	17.05	4.22	35.31	16.19	26.61	1.99	33.11	19.04	24.50	26.40
TiO_2	0.12	1.34	1.75	0.27	b.d.	3.17	0.06	0.06	0.04	b.d.	0.08	0.06
FeO*	12.76	17.21	18.07	12.03	1.28	16.23	3.11	15.62	2.51	13.25	10.49	3.40
Cr_2O_3	0.08	b.d.	0.06	0.12	0.07	0.10	0.07	0.07	b.d.	0.23	0.07	b.d.
MnO	0.41	0.23	0.19	0.77	0.10	0.32	0.12	0.36	0.06	0.28	0.13	0.17
MgO	14.30	11.63	10.87	15.02	1.03	11.87	2.07	13.26	1.84	25.08	b.d.	1.80
CaO	12.56	4.10	0.07	11.54	0.14	0.05	21.54	12.44	b.d.	0.04	23.03	22.00
Na_2O	0.26	0.14	0.08	0.32	b.d.	b.d.	b.d.	0.26	0.16	b.d.	b.d.	b.d.
K_2O	0.20	6.46	9.67	0.12	10.39	9.23	0.11	0.09	8.89	b.d.	b.d.	0.08
Sum	97.38	95.14	94.03	96.46	95.98	93.74	91.27	97.86	9.54	87.63	96.42	92.02
Si	7.63	3.09	2.78	7.49	3.11	2.85	6.09	7.82	3.16	2.93	3.03	6.13
Al^{IV}	0.37	0.91	1.22	0.52	0.89	1.15	n.c.	0.18	0.84	1.07	0.00	n.c.
Al^{VI}	0.31	0.19	0.33	0.20	1.82	0.35	5.08	0.16	1.68	1.15	2.29	5.01
Ti	0.01	0.07	0.10	0.03	b.d.	0.19	0.01	0.01	0.00	b.d.	0.00	0.01
Fe^{3+}	0.05	0.61	0.95	0.58	0.07	0.00	0.00	0.03	0.14	0.00	0.70	0.00
Cr	0.01	b.d.	0.00	0.01	0.00	0.01	0.01	0.01	b.d.	0.02	0.00	b.d.
Fe^{2+}	1.49	0.46	0.21	0.87	0.00	1.06	0.42	1.88	0.00	1.10	0.00	0.46
Mn	0.05	0.01	0.01	0.09	0.01	0.02	0.02	0.04	0.00	0.02	0.01	0.02
Mg	3.08	1.29	1.25	3.22	0.10	1.38	0.50	2.88	0.18	3.70	b.d.	0.43
Ca	1.95	0.33	0.01	1.78	0.01	0.00	3.74	1.94	b.d.	0.00	1.96	3.79
Na	0.08	0.02	0.01	0.09	b.d.	b.d.	b.d.	0.07	0.02	b.d.	b.d.	b.d.
K	0.02	0.61	0.95	0.02	0.86	0.92	0.02	0.02	0.73	b.d.	b.d.	0.02

Red Ant terrane, pumpellyite-actinolite facies sample M5e							Feather River terrane, sample M119		
Mineral	Act	Chl	Mu	Bio	Pmp	Lws	Act	Pmp	Mu
SiO_2	52.21	28.80	54.30	33.97	37.13	40.60	52.67	37.64	57.15
Al_2O_3	2.77	16.99	22.59	17.68	24.84	31.13	0.29	24.74	20.79
TiO_2	0.06	b.d.	0.14	2.94	b.d.	b.d.	0.06	0.15	0.03
FeO*	16.55	28.80	5.39	22.13	5.75	0.15	22.91	4.33	4.44
Cr_2O_3	b.d.	0.04	0.04	b.d.	0.05	b.d.	0.04	b.d.	b.d.
MnO	0.25	0.30	0.03	0.25	0.11	b.d.	0.26	0.06	b.d.
MgO	12.58	13.86	4.51	10.40	2.05	b.d.	8.83	2.52	5.06
CaO	12.25	0.13	0.07	0.05	22.54	16.45	12.10	21.80	0.10
Na_2O	0.54	b.d.	b.d.	b.d.	b.d.	b.d.	0.08	b.d.	0.37
K_2O	0.16	b.d.	10.50	7.13	b.d.	b.d.	0.12	b.d.	9.49
Sum	97.37	88.92	97.31	94.55	92.47	88.33	97.40	91.29	97.45
Si	0.69	3.06	3.52	2.61	6.02	2.11	7.99	6.12	3.69
Al^{IV}	0.32	0.94	0.48	1.39	n.c.	n.c.	0.01	n.c.	0.31
Al^{VI}	0.17	1.20	1.26	0.21	4.75	1.90	0.04	4.75	1.27
Ti	0.01	b.d.	0.01	0.17	b.d.	b.d.	0.01	0.02	0.00
Fe^{3+}	0.09	0.00	0.20	0.00	n.c.	n.c.	0.00	n.c.	0.04
Cr	b.d.	0.00	0.00	b.d.	0.01	0.01	0.01	b.d.	b.d.
Fe^{2+}	1.95	2.56	0.09	1.42	0.49	b.d.	2.91	0.38	0.20
Mn	0.03	0.03	0.00	0.02	0.01	b.d.	0.03	0.01	b.d.
Mg	2.76	2.20	0.44	1.19	0.50	b.d.	2.00	0.61	0.49
Ca	1.93	0.01	0.00	0.00	3.92	0.91	1.97	3.79	0.01
Na	0.16	b.d.	b.d.	b.d.	b.d.	b.d.	0.02	b.d.	0.05
K	0.03	b.d.	0.87	0.70	b.d.	b.d.	0.02	b.d.	0.78

Mineral abbreviations explained in Table 1. Formulae were calculated following the method of Laird and Albee (1981), except that pumpellyite cations are averages of calculations assuming that all iron is ferric and assuming that all iron is ferrous. "n.c.": cations not calculated, either Al coordination or Fe valence. "b.d.": below detection. See Hacker and Goodge (1990) for analyses of blueschist-facies rocks in the Red Ant terrane.

pyroxene, similar to assemblages reported for the Shuksan metamorphic suite (Brown, 1977b), Condrey Mountain schist and Pickett Peak terrane, northern California (Brown and Blake, 1987), and the Bessi (Banno, 1964) and Shirataki (Seki and others, 1969) districts of the Sanbagawa Belt, Japan.

Various workers have attempted to determine the reaction relationships among the minerals of the pumpellyite-actinolite and related low-grade facies by evaluating naturally occurring parageneses, thermodynamic data, and experimental work. Unfortunately, metamorphic pressures and temperatures are difficult to determine for natural low-grade assemblages, and experimental work on iron-bearing systems has not yet progressed to where equilibrium conditions of reactions are known. Inferences can be drawn from iron-free experiments and thermodynamic calculations, but they are necessarily qualitative.

As many as 14 metamorphic minerals are present in samples from the Yuba River area, although most samples contain only 7 or 8. These minerals can be described by the following 13 components: SiO_2, TiO_2, Al_2O_3, Fe_2O_3, FeO, MnO, MgO, CaO, Na_2O, K_2O, SO_2, H_2O, and CO_2. The number of components can be reduced to four: Al_2O_3, Fe_2O_3, (Fe,Mg,Mn)O, and CaO, if we consider that (1) SiO_2, TiO_2, Na_2O, K_2O, and SO_2 are retained in quartz, sphene, albite, phengite, and sulfide minerals, respectively; (2) FeO, MgO, and MnO are equivalent components in solid solutions (but see Springer and others, 1992); and (3) H_2O and CO_2 are excess or mobile components (Zen, 1974). Eight phases in this reduced, four-component system are found in the Yuba River area: epidote, lawsonite, pumpellyite, actinolite, chlorite, sodic amphibole, hematite, and magnetite. In a four-component system, an assemblage of four phases is divariant with respect to pressure and temperature, a five-phase assemblage is univariant, and six phases form an invariant assemblage. Figure 12 illustrates phase assemblages and compositions in the Yuba River area using the components Al, Ca, Fe^{3+}, and Fe^{2+}+Mg. Except for iron oxide, all phases lie on or near the Al-Ca-Fe^{2+}+Mg face of the tetrahedron. To illustrate the variable Fe^{3+} contents of the phases, the mineral compositions are projected from an average chlorite composition onto the plane shown. The assemblage epidote + actinolite + iron oxide is widespread and contains the most Fe-rich epidote. Fe-poor epidote coexists with pumpellyite + actinolite, a compatible assemblage. In the presence of chlorite, epidote + actinolite are incompatible with pumpellyite + iron oxide. These two groups of assemblages define the reaction epidote + actinolite = pumpellyite + iron oxide.

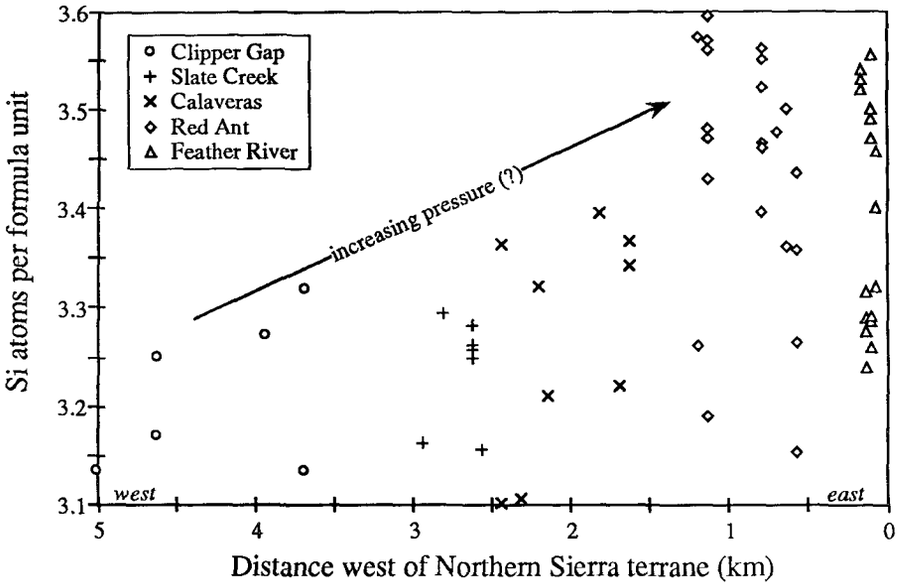

Figure 11. The maximum Si content of K-white mica generally increases eastward, although it may peak in the Red Ant terrane.

Assemblages in the Yuba River area can be related to one another by the reactions shown in Figure 13, adapted from Brown (1977a) and Liou and others (1987). The sodic amphibole + lawsonite assemblages reported by Schweickert and others (1980), and the epidote rims on lawsonite coexistent with pumpellyite found in this study make it likely that a reaction similar to sodic amphibole + lawsonite → epidote + pumpellyite took place (reaction 1; Fig. 13). Similarly, the pumpellyite + actinolite + epidote assemblages grown over sodic amphibole + epidote assemblages may have formed by reactions 2 and 3 in Figure 13. An alternative path, via reactions 4 and 5, is less likely because sodic amphibole + pumpellyite + iron oxide parageneses are absent from the Red Ant terrane.

Reaction 5, pumpellyite + iron oxide → epidote + actinolite, is preserved in rocks in the Yuba River area containing the reaction assemblage pumpellyite + iron oxide + epidote + actinolite. No systematic regional distribution of reactant assemblages relative to product assemblages can be discerned in Figure 2B, and an isograd separating the assemblages cannot be drawn. Hence, all three of these terranes are essentially isofacial, although not necessarily isophysical. The same reaction has been suggested by Seki (1961), Hashimoto (1972), and Nakajima and others (1977) to separate subzones of pumpellyite-actinolite–facies rocks.

The metamorphic pressures and temperatures recorded in the Yuba River area increase from west to east. This metamorphic field gradient generally is not observed within individual units, but is marked by changes in metamorphic parageneses from one unit to the next (Fig. 2B). The Clipper Gap Formation is only incipiently recrystallized and generally lacks pumpellyite, whereas all other units contain pumpellyite. This change is nearly coincident with the contact between the Clipper Gap Formation and the Slate Creek terrane, which is a steeply east-dipping reverse fault (Edelman and others, 1989b). Lawsonite and sodic amphibole are found only in the Red Ant terrane. The boundaries defining lawsonite-bearing and sodic-amphibole–bearing assemblages are coincident with the contact between the Red Ant and Feather River terranes, which has been interpreted as a west-directed thrust fault placing the Feather River terrane over the Red Ant terrane (Edelman and others, 1989b). Thus, all three of these pseudo-isograds ("pumpellyite in," "lawsonite out," and "sodic amphibole out") nearly coincide with faults. The appearance of pumpellyite is not an isograd in the proper sense because it is limited by the degree of recrystallization. Textures described above indicate that the "lawsonite out," and "sodic amphibole out" boundaries result from pumpellyite-actinolite–facies overprinting of blueschist-facies assemblages.

Using coexisting phases and phase compositions, Hacker and Goodge (1990) estimated metamorphic pressures and temperatures of 500–700 MPa and 250–400 °C for crossite-epidote assemblages, 500–700 MPa and 200–300 °C for glaucophane-lawsonite–bearing rocks in the Red Ant terrane, and 200–400 MPa and 150–350 °C for more widespread pumpellyite-actinolite assemblages. The absolute numbers are not as important as the observation that the pumpellyite-actinolite–facies metamorphism may be of the high- to moderate-pressure–facies series, and does not represent low-pressure–facies series metamorphism. Quartz microstructures suggest an eastward increase in metamorphic temperatures, ranging from solution cleavage and cracking in the Clipper Gap to dislocation creep in the Red Ant terrane. An eastward increase in metamorphic temperatures is also compatible with the eastward increase in density and spacing of quartz veins in sedimentary rocks. Metamorphic pressure may increase from west to east, based on the eastward increase in phengite silica content (Fig. 11).

Timing of Magmatism, Deformation, and Metamorphism

A prerequisite to deciphering continental growth in the Sierra Nevada is understanding the timing of depositional, magmatic, deformational, and metamorphic events. It is clear that most tectonism occurred in Mesozoic time, but new constraints allow more precise resolution (Fig. 14).

A range of Devonian to Permian K/Ar and Ar/Ar hornblende ages indicates that amphibolite-facies metamorphism in the Feather River terrane was diachronous (Hacker and Peacock, 1990). The timing of the later pumpellyite-actinolite–facies metamorphism in the Feather River terrane is not well constrained, although it clearly postdates Permian amphibolite-facies metamorphism. Rosenbaum (in Day and others, 1988) reported that pumpellyite-bearing veins predate Early Cretaceous quartz-sulfide-gold(?) veins dated as ~113 Ma by Böhlke and McKee (1984) using the K/Ar method. The only possible direct date of the pumpellyite-actinolite–facies metamorphism in the Feather River terrane is a 166 Ma Pb/U age obtained by Saleeby and others (1989) on metamorphic sphene, which is a widespread component of the pumpellyite-actinolite–facies parageneses. Deformation coincident with pumpellyite-actinolite–facies metamorphism in this terrane is limited to distributed cracking and veining; no penetrative foliation or lineation developed.

Blueschist-facies metamorphism in the Red Ant terrane was accompanied by, and

TABLE 4. ANALYSES OF STILPNOMELANE FROM THE RED ANT TERRANE

Sample	M21	RR1	M77
SiO_2	47.07	48.64	48.07
Al_2O_3	6.07	5.41	6.04
TiO_2	b.d.	b.d.	b.d.
FeO*	28.56	24.40	28.08
Cr_2O_3	b.d.	0.10	0.02
MnO	0.79	2.87	0.91
MgO	5.01	7.90	6.58
CaO	0.11	0.35	0.26
Na_2O	b.d.	b.d.	b.d.
K_2O	0.63	0.46	0.59
Sum	88.24	90.13	90.55
Si	8.00	8.00	8.00
Al	1.22	1.05	1.19
Ti	b.d.	b.d.	b.d.
Cr	b.d.	0.00	0.00
Fe*	4.06	3.36	3.91
Mn	0.11	0.40	0.13
Mg	1.27	1.94	1.63
Ca	0.02	0.06	0.05
Na	b.d.	b.d.	b.d.
K	0.14	0.10	0.13

followed by, fracturing, crystal-plastic deformation of albite and quartz, and ptygmatic folding. Pumpellyite-actinolite–facies metamorphism occurred later, concomitant with fracturing, local folding, and extensive crystal-plastic deformation of calcite, albite, and quartz. K/Ar whole-rock and muscovite ages reported by Schweickert and others (1980) are Early to Middle Jurassic, but such dates are difficult to interpret (Wijbrans and McDougall, 1986). The absolute metamorphic age is unknown, and there is no measure of how much time, if any, elapsed between the growth of the blueschist and pumpellyite-actinolite mineral assemblages. Correlation of the Red Ant terrane with the more precisely dated Stuart Fork terrane in the Klamath Mountains (Hacker and Goodge, 1990) suggests that the blueschist-facies metamorphism may be ~219 Ma. The pumpellyite-actinolite–facies recrystallization consequently must be younger.

Sedimentation in the Calaveras terrane must have occurred, at least in part, after Permian time because the unit contains carbonate blocks with Permian fossils (Hietanen, 1981; Standlee and Nestell, 1985). Radiolaria in chert indicate deposition in Late Triassic time and even younger metamorphism.

The Slate Creek terrane formed during Late Triassic time (209–202 Ma; Edelman and others, 1989a; Saleeby and others, 1989). The Bloody Run pluton (Fig. 2A) cuts foliation in the Slate Creek and Clipper Gap units, constraining significant deformation and metamorphism of the host units to pre–165 Ma. Isofacial metamorphic assemblages in the deformed Bloody Run pluton and its host rocks suggest that some metamorphism and deformation of the pluton and host rocks might partially postdate 165 Ma. The Calaveras and Slate Creek terranes both contain syntectonic pumpellyite-actinolite assemblages and a similar crenulation cleavage, suggesting that metamorphism and deformation were synchronous in both units, beginning before 165 Ma, but possibly continuing to a slightly younger date.

Several ages constrain timing of events in the Clipper Gap Formation. Fossils from bedded strata yield Middle Triassic and Late Triassic–Early Jurassic ages (Irwin and others, 1978; Hietanen, 1981). The structurally lowest part of the Clipper Gap is deposited on the Owl Gulch volcanics. At Jarbo Gap, 40 km northwest of the study area, plutonic and hypabyssal rocks that are possibly correlative with the Owl Gulch volcanics (Dilek, 1989) yield Pb/U and Sm/Nd ages of ~205 Ma (Saleeby and others, 1989). Deposition of the

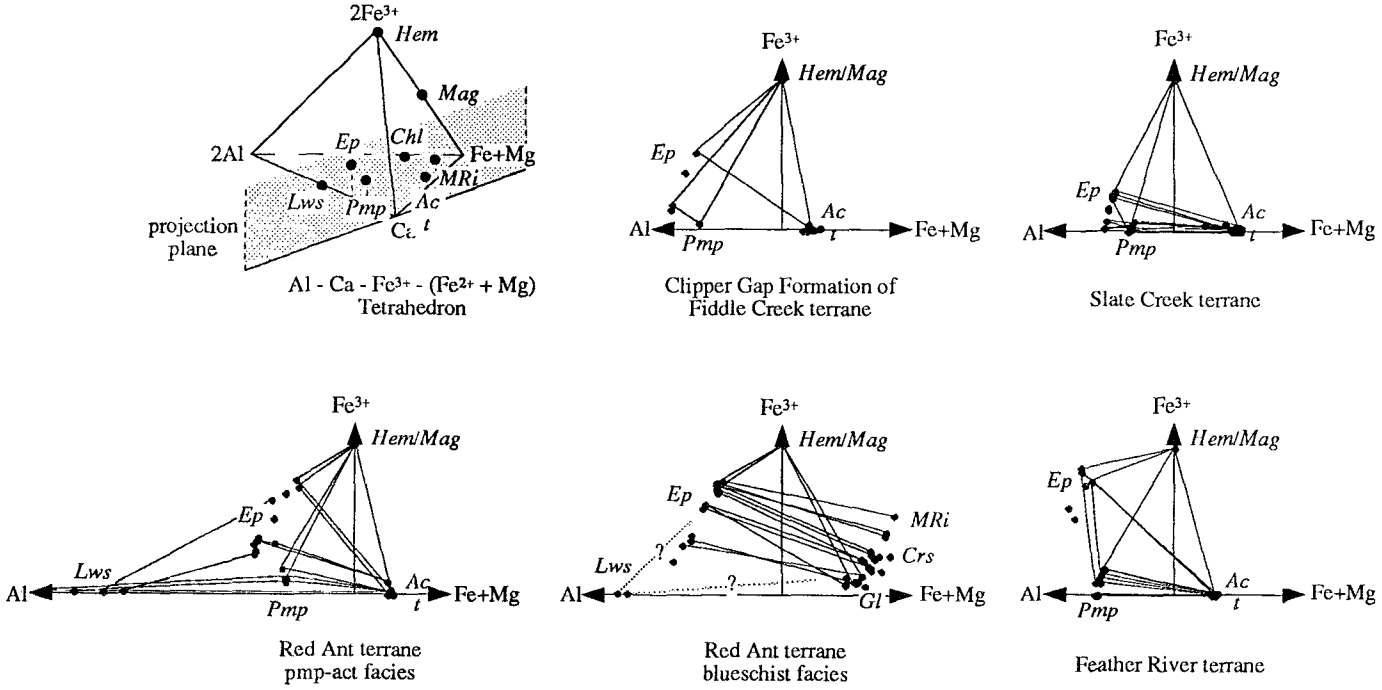

Figure 12. Compositions of pumpellyite-actinolite and blueschist-facies minerals coexisting with chlorite, quartz, albite, phengite, sphene, and iron oxide in volcanic and volcanogenic lithologies. The phases are shown projected from $(Mg,Fe)_{5.5}Al_{0.5}Si_{3.0}Al_{1.0}O_{10}(OH)_8$ chlorite onto a plane normal to the Al-Ca join of an Al-Ca-Fe^{3+}-(Fe^{2+}+Mg) tetrahedron (similar to Liou and others, 1987). This chlorite composition is intermediate among the chlorites from the Yuba River area; changes in chlorite composition affect scaling of the axes, but do not affect the graphical relationships among the phases. This projection illustrates the $Fe^{3+} \leftrightarrow$ Al substitution in Ca-Al silicates and the compositional differences between sodic and calcic amphibole. Ep: epidote; Act: actinolite; Pmp: pumpellyite; Lws: lawsonite; MRi: magnesio-riebeckite; Crs: crossite; Gl: glaucophane. Pumpellyite Fe^{3+}/Fe^{2+} calculated from $Fe^{2+} = 1 - Mg$ (after Brown and Ghent, 1983), but see discussion in text.

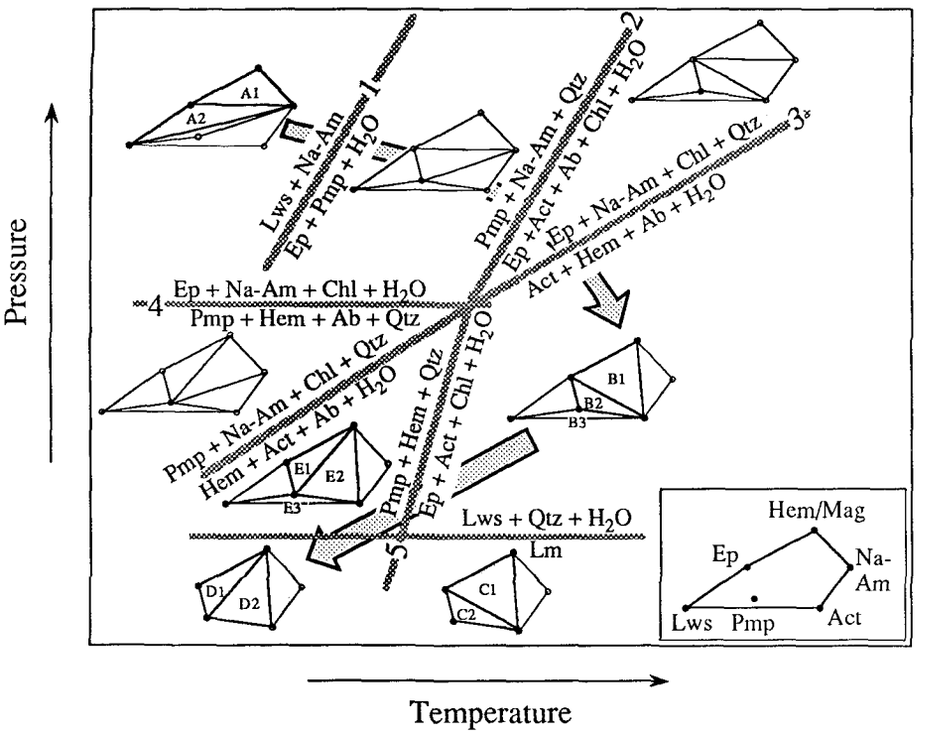

Figure 13. Schematic relationships among mineral assemblages in the Yuba River area, after Brown (1977b), Brown and Ghent (1983), Brown and Blake (1987), and Liou and others (1987). Lettered assemblages occur in the Yuba River area and correspond to Table 1. Labeled reactions are discussed in the text. Assemblages "B" and "C," and "D" and "E" cannot be distinguished from each other, except by the presence or absence of lawsonite, which may be controlled by bulk composition. Abbreviations as per Table 1; "Lm": laumontite. Arrows show possible pressure-temperature path.

structurally lowest part of the Clipper Gap may thus be Late Triassic or younger. The presence of Middle Triassic chert in structurally higher parts of the Clipper Gap implies the presence of intraterrane thrust faults, a reasonable feature in an accretionary wedge. Volcanic hornblende crystals separated from a boulder in the lahar at Edwards Crossing yielded a $^{40}Ar/^{39}Ar$ age of 174 Ma (Fig. 10). An exotic metasedimentary block in the Clipper Gap yielded a probable amphibolite-facies metamorphic age of ~350 Ma; this age and the high-temperature mineral paragenesis suggest that the block was derived from the Feather River terrane. Deposition was finished by Middle Jurassic time as signaled by intrusion of the 168-m.y.-old Scales pluton (5 km north of the study area), the 165-m.y.-old Bloody Run tonalite (Fig. 10), and the 159-m.y.-old Yuba Rivers pluton (Fig. 2A) (Edelman and others, 1989a; Saleeby and others, 1989). Foliation formation postdated deposition of the 174 Ma lahar and mostly predated the 165 Ma Bloody Run tonalite. The Yuba Rivers pluton is not metamorphosed, and it postdates mafic dikes in the Clipper Gap Formation. Thus deposition of the Clipper Gap Formation was active in Middle Triassic and continued through Middle Jurassic time. Weak regional metamorphism, penetrative deformation, and mafic dike intrusion must have occurred between 174 and 165 Ma.

In summary, deformation and low-temperature metamorphism in the Yuba River area may have occurred in the 174–160 Ma time frame in all units, or it may have swept diachronously from east to west.

Tectonic Implications

Schweickert and others (1980) concluded that the blueschist-facies parageneses in the Red Ant terrane formed in a subduction zone. The pumpellyite-actinolite–facies metamorphism in the Red Ant may have developed immediately after the blueschist-facies metamorphism while the same tectonic processes were active. If so, the rocks decompressed in a clockwise path during the blueschist- to pumpellyite-actinolite–facies transition. The pumpellyite-actinolite–facies metamorphism developed at moderate to high pressure/temperature conditions, making it difficult to ascribe to a specific tectonic environment. The metamorphic conditions are compatible with the deeper levels of a magmatic arc or the shallower levels of an accretionary wedge—they are not compatible with ocean-ridge hydrothermal activity or heating in the upper levels of a magmatic arc. Moreover, there is no indication that plutons currently exposed in the Yuba River area caused the observed regional distribution of parageneses.

The Calaveras and Clipper Gap units have been interpreted as west-vergent accretionary complexes based on the pervasive mixing of different rock types (for example, Hietanen, 1981; Schweickert and others, 1988; Sharp, 1988). These units and the Red Ant terrane contain similar protoliths and exhibit moderate- to high-pressure parageneses; they differ most in their deformation fabrics. They may represent three temporally successive parts of an accretionary wedge formed during east-dipping subduction. Such an interpretation is supported by the eastward increase in inferred metamorphic temperatures, pressures, and degree of deformation. The ages of metamorphism may also increase eastward.

A different scenario, also supported by existing data, is that the pumpellyite-actinolite–facies metamorphism significantly postdated the blueschist-facies metamorphism and was synchronous in all units between 174 and 165 Ma. Deformation may also have been synchronous across the Yuba River area, and instead of relating to potentially long-lived subduction, may have resulted from more rapid closure of intra-arc basins.

Although the Late Jurassic Nevadan orogeny is often considered responsible for much of the structural expression of the range (see Schweickert and others, 1984), older and younger episodes of metamorphism and deformation had important effects in the Sierra Nevada (Schweickert and others, 1988; Day and others, 1988; Tobisch and others, 1989). In the Yuba River area, Middle Jurassic(?) orogeny produced widespread recrystallization and deformation. Considerable Late Jurassic orogenesis may have occurred there, but the metamorphic and deformational aspects of this event are not clearly separable from older tectonism. If, for instance, the Nevadan orogeny in the Yuba River area occurred at temperatures too low for growth of diagnostic or datable metamorphic minerals,

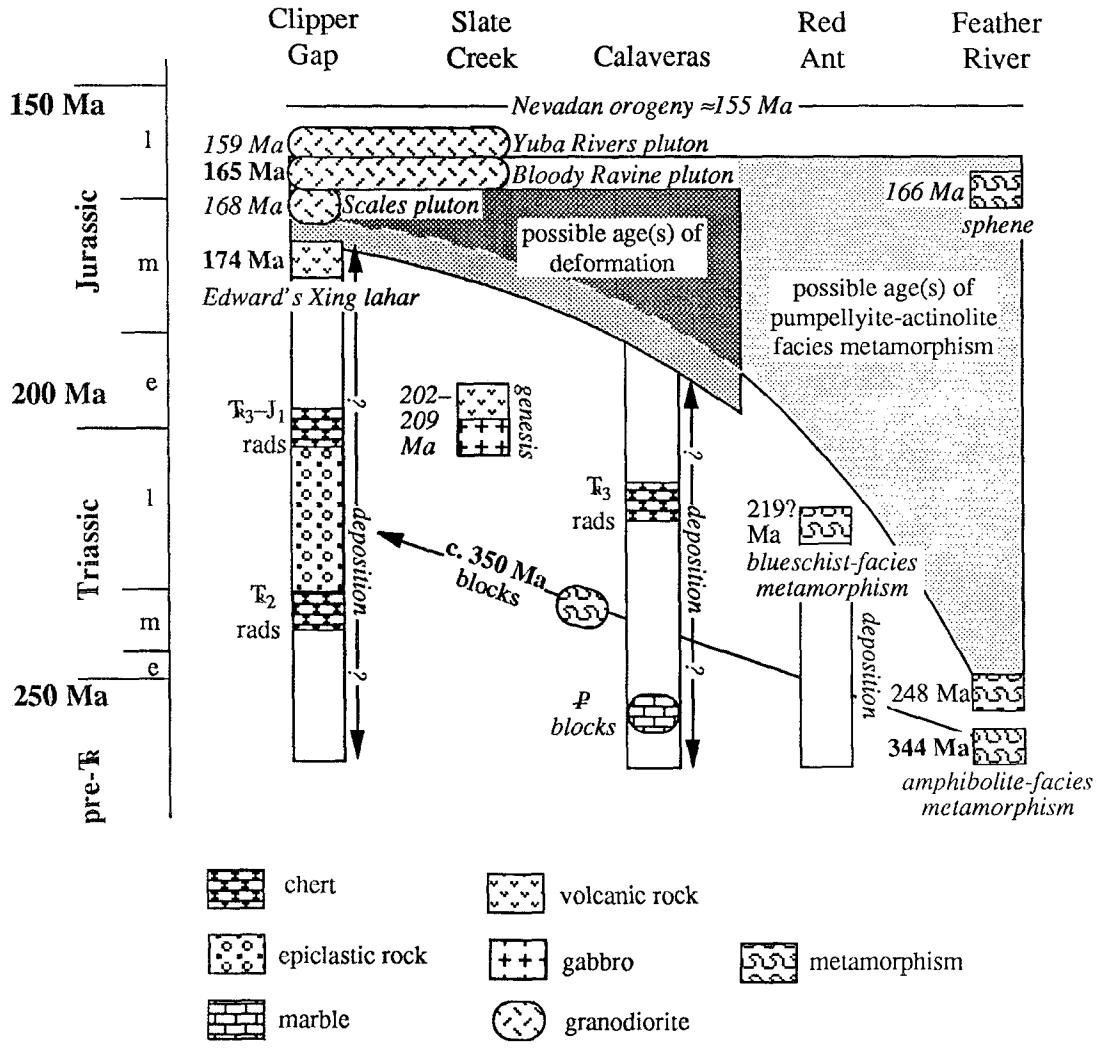

Figure 14. Timing relationships in the Yuba River area. Unfilled vertical columns illustrate potential range of depositional ages. Shaded areas show potential times of deformation and pumpellyite-actinolite–facies metamorphism. Ar/Ar ages from this study are in boldface. Pb/U ages (Edelman and others, 1989; Saleeby and others, 1989) are italicized. The ~219? Ma age shown for Red Ant terrane is derived from the probably correlative Stuart Fork terrane in the Klamath Mountains (Hacker and Goodge, 1990). Fossil ages are from Irwin and others (1977), Hietanen (1981), and Standlee and Nestell (1985).

it might be difficult to differentiate Nevadan structures from earlier structures.

CONCLUSIONS

This study is a preliminary step toward unraveling the tectonic setting and timing of deposition, magmatism, metamorphism, and deformation in the Yuba River area of the Sierra Nevada metamorphic belt. At this latitude, the belt is an amalgam of deformed, low-grade, oceanic sedimentary and magmatic arc rocks. The largest and westernmost of the sedimentary units, the Clipper Gap, received detritus from diverse sources, including distal and proximal volcanoplutonic arcs, and metamorphosed and unmetamorphosed continental and mafic provenances. Deposition began by Triassic time and continued to at least 174 Ma, the age of volcaniclastic detritus. The presence and age of quartzose detritus and high-grade exotic blocks suggest that the Northern Sierra or Feather River terranes, which lie a few kilometers to the east, may have been one of these sources; thus, the Clipper Gap need not have traveled far. More inboard units were metamorphosed and deformed at higher pressures and temperatures characteristic of pumpellyite-actinolite to blueschist–facies metamorphism. The pumpellyite-actinolite–facies metamorphism was widespread, even involving the easternmost Feather River terrane, a much older part of the orogen against which the younger units formed.

Metamorphic breaks observed across terrane-bounding faults, the paucity of plutonic rocks, and the absence of low-pressure metamorphic assemblages suggest that the pumpellyite-actinolite–facies metamorphism is of regional and not contact type, and that it predates displacements on these faults. The metamorphism may have occurred within the volcanoplutonic arcs that make up much of the orogen, or within related subduction zones, but it did not accompany the intrusion of widespread Jurassic-Cretaceous granodioritic plutons. Pumpellyite-actinolite–facies metamorphism may have occurred synchronously in all units between 174 and 165 Ma, or it may have swept diachronously from east to west. None of the metamorphism described here can be unambiguously attributed to the Nevadan orogeny, which occurred about 10 m.y. later.

ACKNOWLEDGMENTS

Thanks to Robert Jones for microprobe assistance, and H. W. Day, J. L. Mosenfelder, J. G. Liou, and R. A. Schweickert for criticism of the manuscript. This work was sup-

ported by Department of Energy grants DE-FGO3-40ER14154 and 8802-121.

REFERENCES CITED

Aiba, K., 1982, Sanbagawa metamorphism of the Nakatsu-Nanokawa district, the northern sub-belt of the Chichibu belt in western central Shikoku: Geological Society of Japan Journal, v. 88, p. 875–885.

Banno, S., 1964, Petrologic studies on Sanbagawa crystalline schist in the Bessi-Ino district, central Shikoku, Japan: Tokyo University Faculty of Sciences Journal, Section II 15, p. 203–319.

Beard, J. S., and Day, H. W., 1987, The Smartville intrusive complex, Sierra Nevada, California: The core of a rifted volcanic arc: Geological Society of America Bulletin, v. 99, p. 779–791.

Böhlke, J. K., and McKee, E. H., 1984, K/Ar ages relating to metamorphism, plutonism, and gold-quartz vein mineralization near Alleghany, Sierra County, California: Isochron/West, v. 39, p. 3–7.

Brown, E. H., 1971, Phase relations of biotite and stilpnomelane in the greenschist facies: Contributions to Mineralogy and Petrology, v. 31, p. 275–299.

Brown, E. H., 1977a, The crossite content of Ca-amphibole as a guide to pressure of metamorphism: Journal of Petrology, v. 18, p. 53–72.

Brown, E. H., 1977b, Phase equilibria among pumpellyite, lawsonite, epidote and associated minerals in low grade metamorphic rocks: Contributions to Mineralogy and Petrology, v. 64, p. 123–136.

Brown, E. H., and Blake, M. C., Jr., 1987, Correlation of Early Cretaceous blueschists in Washington, Oregon and northern California: Tectonics, v. 6, p. 795–806.

Brown, E. H., and Ghent, E. H., 1983, Mineralogy and phase relations in the blueschist facies of the Black Butte and Ball Rock areas, northern California Coast Ranges: American Mineralogist, v. 68, p. 365–372.

Byrne, T., 1984, Early deformation in melange terranes of the Ghost Rocks Formation, Kodiak Islands, Alaska, *in* Raymond, L. A., ed., Melanges: Their nature, origin and significance: Geological Society of America Special Paper 198, p. 21–51.

Coombs, D. S., Makanura, Y., and Vuagnat, M., 1976, Pumpellyite-actinolite facies schists of the Taveyanne formation near Loèche, Valais, Switzerland: Journal of Petrology, v. 17, p. 440–471.

Cowan, D. S., 1985, Structural styles in Mesozoic and Cenozoic mélanges in the western Cordillera of North America: Geological Society of America Bulletin, v. 96, p. 451–462.

Day, H. W., Schiffman, P., and Moores, E. M., 1988, Metamorphism and tectonics of the northern Sierra Nevada, *in* Ernst, W. G., ed., Metamorphism and crustal evolution of the western United States; Rubey Volume 7: Englewood Cliffs, New Jersey, Prentice-Hall, p. 737–763.

Dilek, Y., 1989, Structure and tectonics of an Early Mesozoic oceanic basement in the northern Sierra Nevada metamorphic belt, California: Evidence for transform faulting and ensimatic arc evolution: Tectonics, v. 8, p. 999–1014.

Edelman, S. H., Day, H. W., and Bickford, M. E., 1989a, Implications of U-Pb zircon ages for the tectonic setting of the Smartville and Slate Creek complexes, northern Sierra Nevada, California: Geology, v. 17, p. 1032–1035.

Edelman, S. H., Day, H. W., Moores, E. M., Zigan, S. M., Murphy, T. P., and Hacker, B. R., 1989b, Structure across a Mesozoic ocean-continent suture zone in the northern Sierra Nevada, California: Geological Society of America Special Paper 224, 56 p.

Evans, B. W., and Patrick, B. E., 1987, Phengite-3T in high-pressure metamorphosed granitic orthogneisses, Seward Peninsula, Alaska: Canadian Mineralogist, v. 25, p. 141–158.

Guidotti, C. V., Post, J. L., and Cheney, J. T., 1979, Margarite pseudomorphs after chiastolite in the Georgetown area, California: American Mineralogist, v. 64, p. 728–732.

Hacker, B. R., 1984, Stratigraphy and structure of the Yuba Rivers area, Central Belt, northern Sierra Nevada, California [M.S. thesis]: Davis, California, University of California, 125 p.

Hacker, B. R., and Goodge, J. W., 1990, Comparison of Mesozoic high-pressure rocks in the Klamath Mountains and Sierra Nevada, *in* Harwood, David S., and Miller, M. Meghan, eds., Paleozoic and Early Mesozoic paleogeographic relations: Sierra Nevada, Klamath Mountains, and related terranes: Geological Society of America Special Paper 255, p. 277–295.

Hacker, B. R., and Peacock, S. M., 1990, Comparison of the Central Metamorphic Belt and Trinity Complex in the Klamath Mountains and the Feather River terrane in the Sierra Nevada: Early to middle Paleozoic tectonism in the Klamath-Sierran Arc, *in* Harwood, David S., and Miller, M. Meghan, eds., Paleozoic and Early Mesozoic paleogeographic relations: Sierra Nevada, Klamath Mountains, and related terranes: Geological Society of America Special Paper 255, p. 75–91.

Hacker, B. R., Ernst, W. G., and Barton, M. D., 1992, Metamorphism, geochemistry and origin of magnesian metavolcanic rocks, Klamath Mountains, California: Journal of Metamorphic Geology, v. 10, p. 55–69.

Harland, W. B., Armstrong, R. L., Cox, A. V., Craig, L. E., Smith, A. G., and Smith, D. G., 1989, A geologic time scale: Cambridge, England, Cambridge University Press, 263 p.

Harwood, D. S., 1988, Tectonism and metamorphism in the northern Sierra terrane, northern California, *in* Ernst, W. G., ed., Metamorphism and crustal evolution of the western United States; Rubey Volume 7: Englewood Cliffs, New Jersey, Prentice-Hall, p. 764–788.

Hashimoto, M., 1972, Reactions producing actinolite in basic metamorphic rocks: Lithos, v. 5, p. 19–31.

Hietanen, A., 1974, Amphibole pairs, epidote minerals, chlorite, and plagioclase in metamorphic rocks, northern Sierra Nevada, California: American Mineralogist, v. 59, p. 22–40.

Hietanen, A., 1981, Geology west of the Melones fault between the Feather and North Yuba Rivers California: U.S. Geological Survey Professional Paper 920, 30 p.

Hodych, J. P., and Dunning, G. R., 1992, Did the Manicouagan impact trigger end-of-Triassic mass extinction?: Geology, v. 20, p. 51–54.

Irwin, W. P., Jones, D. L., and Kaplan, T. A., 1978, Radiolarians from pre-Nevadan rocks of the Klamath Mountains, California and Oregon, *in* Howell, D. G., and McDougall, K. A., eds., Mesozoic paleogeography of the western United States: Society of Economic Paleontologists and Mineralogists, Pacific Paleogeography Symposium, Volume 2, p. 303–310.

Ishizuka, H., 1985, Prograde metamorphism of the Horokanai ophiolite in the Kamuikotan Zone, Hokkaido, Japan: Journal of Petrology, v. 26, p. 390–417.

Kawachi, Y., 1975, Pumpellyite-actinolite and contiguous facies metamorphism in part of Upper Wakatipu district, South Island, New Zealand: New Zealand Journal of Geology and Geophysics, v. 18, p. 401–441.

Laird, J., and Albee, A. L., 1981, High-pressure metamorphism in mafic schist from northern Vermont: American Journal of Science, v. 281, p. 97–126.

Liou, J. G., 1979, Zeolite facies metamorphism of basaltic rocks from the East Taiwan ophiolite: American Mineralogist, v. 64, p. 1–14.

Liou, J. G., Maruyama, S., and Cho, M., 1987, Very low-grade metamorphism of volcanic and volcaniclastic rocks—Mineral assemblages and mineral facies, *in* Frey, M., ed., Low temperature metamorphism: Glasgow, Scotland, Blackie, p. 59–112.

McDougall, I., and Harrison, T. M., 1988, Geochronology and thermochronology by the $^{40}Ar/^{39}Ar$ method: New York, Oxford University Press.

Mevel, C., 1981, Occurrence of pumpellyite in hydrothermally altered basalts from the Vema Fracture Zone (Mid-Atlantic Ridge): Contributions to Mineralogy and Petrology, v. 76, p. 386–393.

Nakajima, T., 1982, Phase relations of pumpellyite-actinolite facies metabasites in the Sanbagawa metamorphic belt in central Shikoku, Japan: Lithos, v. 15, p. 267–280.

Nakajima, T., Banno, S., and Suzuki, T., 1977, Reactions leading to the disappearance of pumpellyite in low-grade metamorphic rocks of the Sanbagawa metamorphic belt in central Shikoku, Japan: Journal of Petrology, v. 18, p. 263–284.

Nisbet, E. G., and Pearce, J. A., 1977, Clinopyroxene composition in mafic lavas from different tectonic settings: Contributions to Mineralogy and Petrology, v. 63, p. 149–160.

Passaglia, E., and Gottardi, G., 1973, Crystal chemistry and nomenclature of pumpellyites and julgoldites: Canadian Mineralogist, v. 12, p. 219–223.

Roddick, J. C., 1978, The application of isochron diagrams in ^{40}Ar-^{39}Ar dating: A discussion: Earth and Planetary Science Letters, v. 41, p. 233–244.

Saleeby, J. B., Shaw, H. F., Moores, E. M., and Edelman, S. H., 1989, Pb/U, Sm/Nd and Rb/Sr geochronological and isotopic study of northern Sierra Nevada ophiolitic assemblages, California: Contributions to Mineralogy and Petrology, v. 102, p. 205–220.

Schiffman, P., and Liou, J. G., 1983, Synthesis of Fe-pumpellyite and its stability relations with epidote: Journal of Metamorphic Geology, v. 1, p. 91–101.

Schweickert, R. A., 1981, Tectonic evolution of the Sierra Nevada range, *in* Ernst, W. G., ed., The geotectonic development of California; Rubey Volume 1: Englewood Cliffs, New Jersey, Prentice-Hall, p. 132–181.

Schweickert, R. A., and Cowan, D. S., 1975, Early Mesozoic tectonic evolution of the western Sierra Nevada, California: Geological Society of America Bulletin, v. 86, p. 1329–1336.

Schweickert, R. A., Armstrong, R. L., and Harakal, J. E., 1980, Lawsonite blueschist in the northern Sierra Nevada, California: Geology, v. 8, p. 27–31.

Schweickert, R. A., Bogen, N. L., Girty, G. H., Hanson, R. E., and Merguriam, C., 1984, Timing and expression of the Nevadan orogeny, Sierra Nevada, California: Geological Society of America Bulletin, v. 95, p. 967–979.

Schweickert, R. A., Merguriam, C., and Bogen, N. L., 1988, Deformational and metamorphic history of Paleozoic and Mesozoic basement terranes in the western Sierra Nevada metamorphic belt, *in* Ernst, W. G., ed., Metamorphism and crustal evolution of the western United States; Rubey Volume 7: Englewood Cliffs, New Jersey, Prentice-Hall, p. 789–822.

Seki, Y., 1961, Pumpellyite in low-grade metamorphism: Journal of Petrology, v. 2, p. 407–423.

Seki, Y., Ernst, W. G., and Onuki, H., 1969, Phase proportions and physical properties of minerals and rocks from the Franciscan and Sanbagawa metamorphic terranes: Supplement to Geological Society of America Memoir 124.

Sharp, W. D., 1988, Pre-Cretaceous crustal evolution in the Sierra Nevada region, California, *in* Ernst, W. G., ed., Metamorphism and crustal evolution of the western United States; Rubey Volume 7: Englewood Cliffs, New Jersey, Prentice-Hall, p. 823–864.

Springer, R. K., Day, H. W., and Beiersdorfer, R. E., 1992, Prehnite-pumpellyite to greenschist facies transition, Smartville complex, near Auburn, California: Journal of Metamorphic Geology, v. 10, p. 147–170.

Standlee, L. A., 1978, Middle Paleozoic ophiolite in the Melones fault zone, northern Sierra Nevada, California: Geological Society of America Abstracts with Programs, v. 10, p. 148.

Standlee, L. A., and Nestell, M. K., 1985, Age and tectonic significance of terranes adjacent to the Melones fault zone, N. Sierra Nevada, California: Geological Society of America Abstracts with Programs, v. 17, p. 410.

Tobisch, O. T., Paterson, S. R., Saleeby, J. B., and Geary, E. E., 1989, Nature and timing of deformation in the Foothills terrane, central Sierra Nevada: Its bearing on orogenesis: Geological Society of America Bulletin, v. 101, p. 401–413.

Wijbrans, J. R., and McDougall, I., 1986, $^{40}Ar/^{39}Ar$ dating of white micas from an Alpine high-pressure metamorphic belt on Naxos (Greece): The resetting of the argon isotopic system: Contributions to Mineralogy and Petrology, v. 93, p. 187–194.

Yoshiasa, A., and Matsumoto, T., 1985, Crystal structure refinement and crystal chemistry of pumpellyite: American Mineralogist, v. 70, p. 1011–1019.

Zen, E-An, 1974, Prehnite- and pumpellyite-bearing mineral assemblages, west side of Appalachian metamorphic belt, Pennsylvania to Newfoundland: Journal of Petrology, v. 15, p. 197–242.

MANUSCRIPT RECEIVED BY THE SOCIETY APRIL 6, 1992
REVISED MANUSCRIPT RECEIVED AUGUST 27, 1992
MANUSCRIPT ACCEPTED SEPTEMBER 22, 1992

Printed in U.S.A.